Research Square

Preprints are preliminary reports that have not undergone peer review.
They should not be considered conclusive, used to inform clinical practice,
or referenced by the media as validated information.

# Dynamic Tests on a Five-Storey Structural Steel–Reinforced Concrete Hybrid Building

**Alejandro Saenz Calad**

alejandro.saenzcalad@pg.canterbury.ac.nz

University of Canterbury https://orcid.org/0009-0005-1781-6377

**Ke Jiang**

University of Canterbury

**Santiago Pujol**

University of Canterbury

**Alex Shegay**

University of Auckland

**Mojtaba Hosseini**

University of Auckland

**Susumu Takahashi**

Osaka University: Osaka Daigaku

**Yu-Chen Ou**

National Taiwan University

**Fu-Pei Hsiao**

National Cheng Kung University

**Chung-Chan Hung**

National Cheng Kung University

**Pu-Wen Weng**

NCREE: National Applied Research Laboratories National Center for Research on Earthquake Engineering

**Chia-Chen Lin**

NCREE: National Applied Research Laboratories National Center for Research on Earthquake Engineering

**George C. Yao**

National Cheng Kung University

**Wei-Chung Chen**

NCREE: National Applied Research Laboratories National Center for Research on Earthquake Engineering

**Min-Chi Ko**

NCREE: National Applied Research Laboratories National Center for Research on Earthquake Engineering

**Yanuar Haryanto**
NCREE: National Applied Research Laboratories National Center for Research on Earthquake Engineering

**William Pollalis**
Texas A&M University

**Yu-Hsin Cheng**
National Cheng Kung University

**Rajesh Dhakal**
University of Canterbury

**Jitendra Bhatta**
University of Canterbury

**Julian Rincon**
Natural Hazards Commission Toka Tū Ake

---

**Research Article**

**Keywords:** Building irregularity, Global building performance, Hybrid structures, Large-scale dynamic tests, Torsion

**Posted Date:** April 1st, 2026

**DOI:** https://doi.org/10.21203/rs.3.rs-9174263/v1

**License:** This work is licensed under a Creative Commons Attribution 4.0 International License.
Read Full License

---

# Dynamic Tests on a Five-Storey Structural Steel–Reinforced Concrete Hybrid Building

Alejandro Saenz Calad [a*], Ke Jiang [a], Santiago Pujol [a], Alex Shegay [b], Mojtaba Hosseini [b], Susumu Takahashi [c], Yu-Chen Ou [d], Fu-Pei Hsiao [d, e], Chung-Chan Hung [e], Pu-Wen Weng [d], Chia-Chen Lin [d], George C. Yao [d, e], Wei-Chung Chen [d], Min-Chi Ko [d], Yanuar Haryanto [d,e,f], William Pollalis [g], Yu-Hsin Cheng [e], Rajesh Dhakal [a], Jitendra Bhatta [a], Julian Rincon [h]

[a] Department of Civil and Environmental Engineering, University of Canterbury, Christchurch, New Zealand

[b] Department of Civil and Environmental Engineering, University of Auckland, Auckland, New Zealand

[c] Department of Architectural Engineering, University of Osaka, Osaka, Japan

[d] National Center for Research on Earthquake Engineering, National Institutes of Applied Research, Taipei, Taiwan

[e] Department of Civil Engineering, National Cheng Kung University, Tainan, Taiwan

[f] Department of Civil Engineering, Universitas Jenderal Soedirman, Purwokerto, Indonesia

[g] Department of Civil and Environmental Engineering, Texas A&M University, College Station, Texas, United States of America

[h] Natural Hazards Commission Toka Tū Ake, New Zealand

[*] Corresponding author, Email: alejandro.saenzcalad@pg.canterbury.ac.nz

**Abstract:** Hybrid structures, combining reinforced concrete walls and structural steel frames, have become increasingly common in mid-to-high-rise buildings. The stiffness and toughness of reinforced concrete, combined with the high strength-to-weight ratio and rapid construction of steel components, represent the advantages of this design solution. Nevertheless, limited experimental data exist regarding the overall response of hybrid structures to earthquake demands. Additionally, few large-scale dynamic tests have been conducted on buildings with horizontal irregularities arising from uneven stiffness distributions. This study, conducted through a joint research program between the National Center for

Research on Earthquake Engineering (NCREE) and New Zealand's Centre for Earthquake Resilience QuakeCoRE, presents the results of 42 simulated earthquake tests on a five-storey structural steel–reinforced concrete hybrid building with horizontal irregularities. Two building configurations (braced and unbraced) were tested to investigate the effect of limiting drift on the seismic response of structural and non-structural elements. Both building configurations exhibited a stable structural response up to roof-drift ratios of approximately 3%. Building torsion generated drift demands in the more flexible façade up to 4 times larger than in the stiffer façade. Drift demands were sensitive to the building configuration used and the shape of the displacement spectrum of the simulated ground motions. Regarding non-structural elements, damage on partition walls was observed but remained easily repairable for storey-drift ratios up to 1%. The response of 'acceleration-sensitive' non-structural elements was not clearly sensitive to the building configuration used.

**Keywords:** Building irregularity; Global building performance; Hybrid structures; Large-scale dynamic tests; Torsion

## 1. Introduction

Hybrid structures combining reinforced concrete (RC) walls and structural steel frames are being used broadly in modern construction. This preference is driven by the stiffness and strength of RC walls and the construction efficiency and high strength-to-weight ratio of steel framing (Pascua, Henry, & Toma, 2023). Following the 2011 Canterbury Earthquakes, a survey of new developments in the Central Business District of Christchurch reported that approximately one-third of 74 new buildings have been constructed using a combination of RC walls and steel frames (Bruneau & MacRae, 2017). Similar design practices have also been documented internationally, particularly for mid- and high-rise buildings (Hou et al., n.d.). Despite the expanding use of these systems, studies investigating their global seismic performance remain limited.

Previous research on hybrid structures has primarily been conducted at the component level, focusing on the capacity of steel frame–RC wall connections. Studies by Hawkins et al. (Hawkins et al., 1980)

and Roeder & Hawkins (Roeder & Hawkins, 1981) identified the failure modes of moment-resisting and pinned steel beam–RC wall connections under monotonic loading, showing that the embedment length of anchors or shear studs embedded in the RC wall controlled the rotational capacity of these connections. Subsequent studies (Liu & Zhou, 2005; Shahrooz et al., n.d., 2004) demonstrated that improved detailing of RC walls and the use of both shear studs and anchors increased the rotational capacity of these connections and prevented brittle failure modes. The effect of RC slabs on the structural performance of steel beam–RC wall connections was investigated by Pascua et al. (Pascua, Henry, Toma, et al., 2023), indicating that coupling between RC slab dowels and steel beams could unintentionally increase rotational stiffness and strength, even if the beam connection was initially designed as pinned.

Previous dynamic tests investigating whole-of-building-performance have mostly focused on regular structures with uniform distributions of stiffness (Abrams & Sozen, 1979; Algan, 1982; Aristizabal-Ochoa & Sozen, 1976; Bonacci, 1989; Cecen, 1979; Lepage, 1996; Shah, 2021; Sozen, 1980). Test results showed that maximum roof-drift ratios (RDR) and storey-drift ratios (SDR) were proportional to the spectrum intensity of the input ground motion, calculated as the area under the velocity spectrum curve between 0.1 and 2.5 sec. (Sozen, 1980). Drift ratios have also been observed to be proportional to peak ground velocity (PGV) (Newmark, 1973).

Healey and Sozen (Healey & Sozen, 1978) and Moehle and Sozen (Moehle & Sozen, 1978, 1980) conducted dynamic tests on small-scale RC structures with vertical stiffness irregularities. The irregularity came from tall first and top storeys and a slender wall with different heights for each specimen. Across these studies, SDR and RDR were also observed to be linearly proportional to PGV. Additionally, for both regular structures and structures with vertical irregularities, seismic drift was observed to be uniform across each storey. In contrast, the seismic response of buildings with plan irregularities is dominated by a coupled torsional–translational or a pure torsional response (Ko & Lee, 2006). Torsion emerges from offsets between the centres of mass and stiffness, which result in drift demands that are not uniform across the plan of the structure. Suzuki, et al. (Suzuki et al., 2021)

conducted dynamic tests on two one-bay by two-bay RC frame structures with a masonry infill wall constructed between two external columns. Displacement demands at the flexible side of the structure were observed to be on average 4 times larger than at the stiffer side. Additional tests were performed after the removal of infill walls, in which the torsional–translational response was still observed because of an irregular distribution of cracking and yielding on the RC elements, suggesting that drift demands of structures with torsional response are sensitive to their displacement history. Although previous studies highlight the complexity of structural irregularities, their effects on the overall seismic response of hybrid buildings remain insufficiently investigated.

Seismic drift has long been recognized as a primary parameter governing both structural and non-structural damage (Pujol et al., 2022; Shah, 2021; Sozen, 1980, 2013). While reducing drift limits can reduce deformation-induced damage, concerns persist that stiffer systems may lead to elevated floor accelerations and therefore high demands on 'acceleration-sensitive' non-structural elements, such as ceilings, sprinkler pipe systems, and furniture. Nonetheless, recent field evidence challenges this notion. Pledger (Pledger, 2025) reviewed post-earthquake survey data from 84 Chilean hospitals and observed that damage to 'acceleration-sensitive' elements occurred far less frequently in wall buildings than in frame buildings, suggesting that higher stiffness does not necessarily amplifies damage on 'acceleration-sensitive' non-structural elements. Despite these insights, quantitative data that link drift limits to the performance of structural and non-structural elements in the context of torsional global response remain scarce.

The present study summarizes the results of large-scale dynamic tests on a five-storey structural steel–RC hybrid building incorporating representative non-structural elements. The design of the structure was governed by 3 main considerations: base-shear strength as determined by limit analysis, drift, and detailing to prevent brittle failure modes obtained from capacity design. In this regard, it was not necessary to define force-reduction factors nor target ductility factors. This research aims to (a) identify the dynamic response of hybrid building systems, (b) evaluate drift demands in structures exhibiting

coupled torsional–translational response, and (c) examine how design drift limits influence the performance of both structural and non-structural elements.

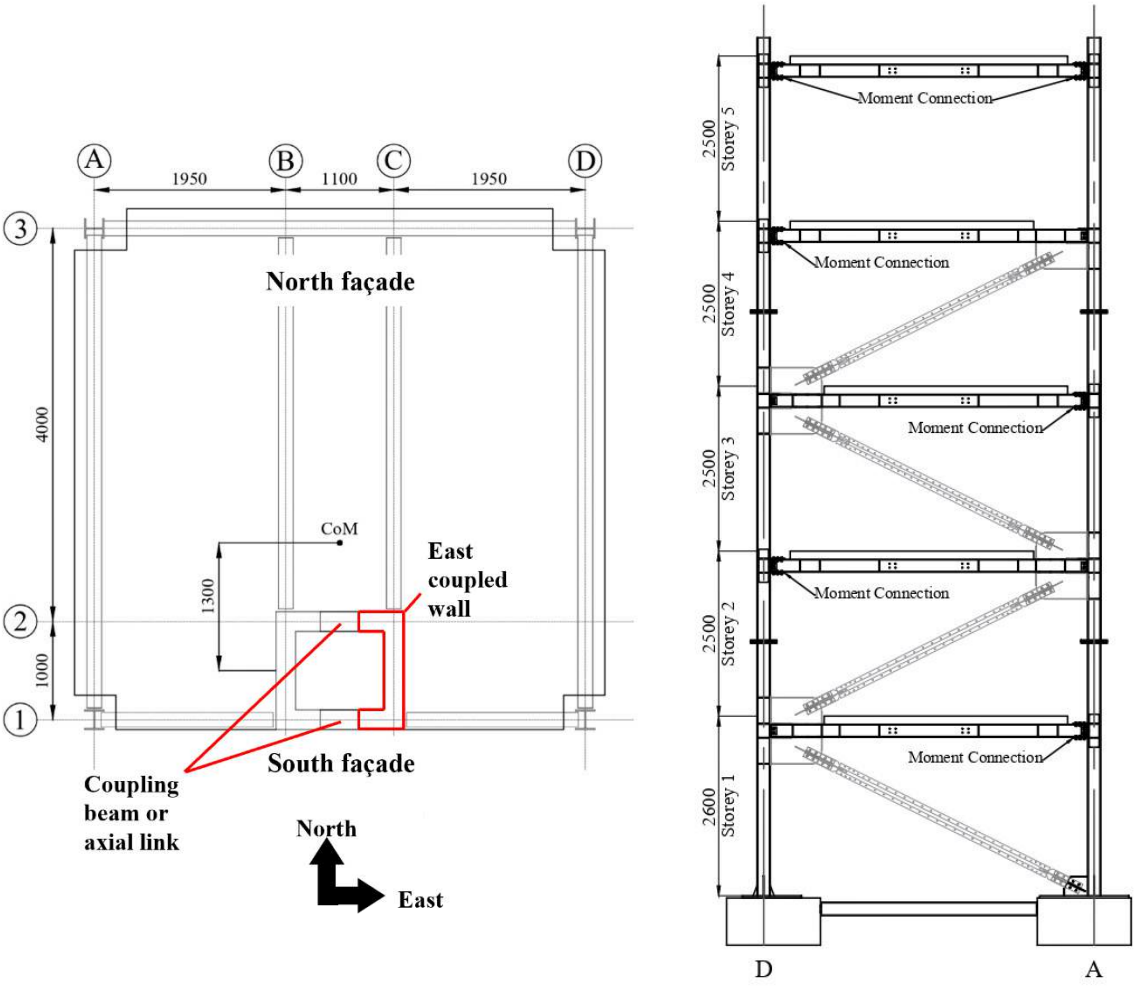
## 2. Test Specimen

### *2.1 Overview of specimen*

The test specimen was a five-storey structural steel–RC hybrid building. Each floor measured 5.4 m × 5.4 m in plan, with typical storey heights of 2.5 m, except for the 1st storey, which had a height of 2.6 m. The total height of the specimen was 12.6 m. A typical floor plan view of the specimen is shown in Fig. 1(a). The centre-to-centre distance between steel columns was 5 m in both north-south (NS) and east-west (EW) directions. The lateral-load-resisting system included 2 RC coupled walls offset 1.3 m from the centre of mass (CoM) in the NS direction, and a structural steel frame. The RC coupled walls provided stiffness and strength in both NS and EW directions, while the steel frame provided lateral stiffness in the EW direction by including moment-resisting connections in alternating joints on grid 3 from the 1st to the 4th storey, and on both beam-column joints in the 5th storey, as shown in Fig. 1(b). Sandwiched buckling-restrained braces (sBRBs) were installed or removed to alter the building configuration in the EW direction. Steel–concrete composite slabs acted as diaphragms transferring inertial forces to the RC wall and steel frame. The building included non-structural components (office furniture, partitions, ceilings, veneers, library shelves, sprinklers, and a curtain wall) amounting to approximately 1 kPa of additional weight per floor except at the roof level.

Because of construction and lifting constraints, the test specimen was fabricated in three independent modules. Each module was first assembled on the strong floor of the laboratory and then lifted onto the top platform of the earthquake simulator. 25-mm thick end plates were used to connect the steel columns of adjacent modules, while 40-mm thick end plates were used to connect adjacent sections of the coupled walls, which were welded to vertical reinforcing bars. End plates were located at mid-height of

the 2nd and 4th storeys. 750-mm tall RC foundation blocks were connected to the bases of each steel column and coupled walls. Casting of the coupled walls, coupling beams, and axial links started with the upper module, followed by the middle module, and ended with the lower module including the foundation blocks. Slabs were casted once each module was assembled.




a) b)

**Fig. 1.** Specimen design (all dimensions in mm): a) typical floor plan, and b) elevation of north façade (grid 3) showing storey heights and locations of moment-resisting connections.

## *2.2 Building configurations*

The building specimen was meant to be representative of new design practices in New Zealand in terms of structural system, design base-shear strength, and initial period. The structure was configured to allow modifications of its stiffness in the EW direction while maintaining a fixed configuration in the

147 NS direction. Tests were completed in three phases, based on the building configuration used. The
148 unbraced configuration was used during phases 1 and 3, while the braced configuration was used during
149 phase 2 (Fig. 2). Calculated story weights of each phase, including both structural and non-structural
150 elements, are summarized in Table 1.
151
152 For the unbraced configuration, lateral resistance in EW direction was provided primarily by the weak
153 axis of the coupled walls and by moment-resisting beam-column connections at grid 3 shown in Fig.
154 1(b). The design roof-drift ratio for this configuration was 2% for a ground motion with PGV
155 approximately equal to 40 cm/s. Calculated initial period for this configuration using gross sections for
156 all RC elements was approximately 0.6 sec. Initial eccentricity for the unbraced configuration,
157 calculated as the distance between the centre of stiffness and the centre of mass ranged between 2% and
158 12% of the building NS plan dimension, depending on assumptions regarding joint connectivity, and
159 composite action of slabs. For the braced configuration, sBRBs and gusset plates were installed on grid
160 3 between storeys 1 to 4. The braces increased the lateral stiffness and strength of the structure in EW
161 direction to achieve a corresponding design roof-drift ratio of 1% for a ground motion with PGV
162 approximately equal to 40 cm/s. Calculated initial period for this configuration using gross sections for
163 all RC elements was approximately 0.4 sec. Initial eccentricity for the braced configuration ranged
164 between 0% and 5%, depending on the same assumptions described above. Lateral resistance for the
165 NS configuration was provided by the strong axis of the coupled-wall system. All connections between
166 steel elements in this direction were detailed as “pinned” connections. Design roof drift ratio for the NS
167 configuration was 1% for a ground motion with PGV approximately equal to 40 cm/s. Calculated initial
168 period for this configuration using gross sections for all RC elements was approximately 0.4 sec.



a) b) c)

**Fig. 2.** Building configurations: a) Phase 1: unbraced configuration, b) Phase 2: braced configuration, c) Phase 3: unbraced configuration.

**Table 1.** Story weights

| Floor | Phase 1 [kN] | Phase 2 [kN] | Phase 3 [kN] |
|---|---|---|---|
| 1 | 156 | 160 | 156 |
| 2 | 154 | 158 | 163 |
| 3 | 155 | 158 | 163 |
| 4 | 154 | 156 | 154 |
| 5 | 112 | 112 | 112 |

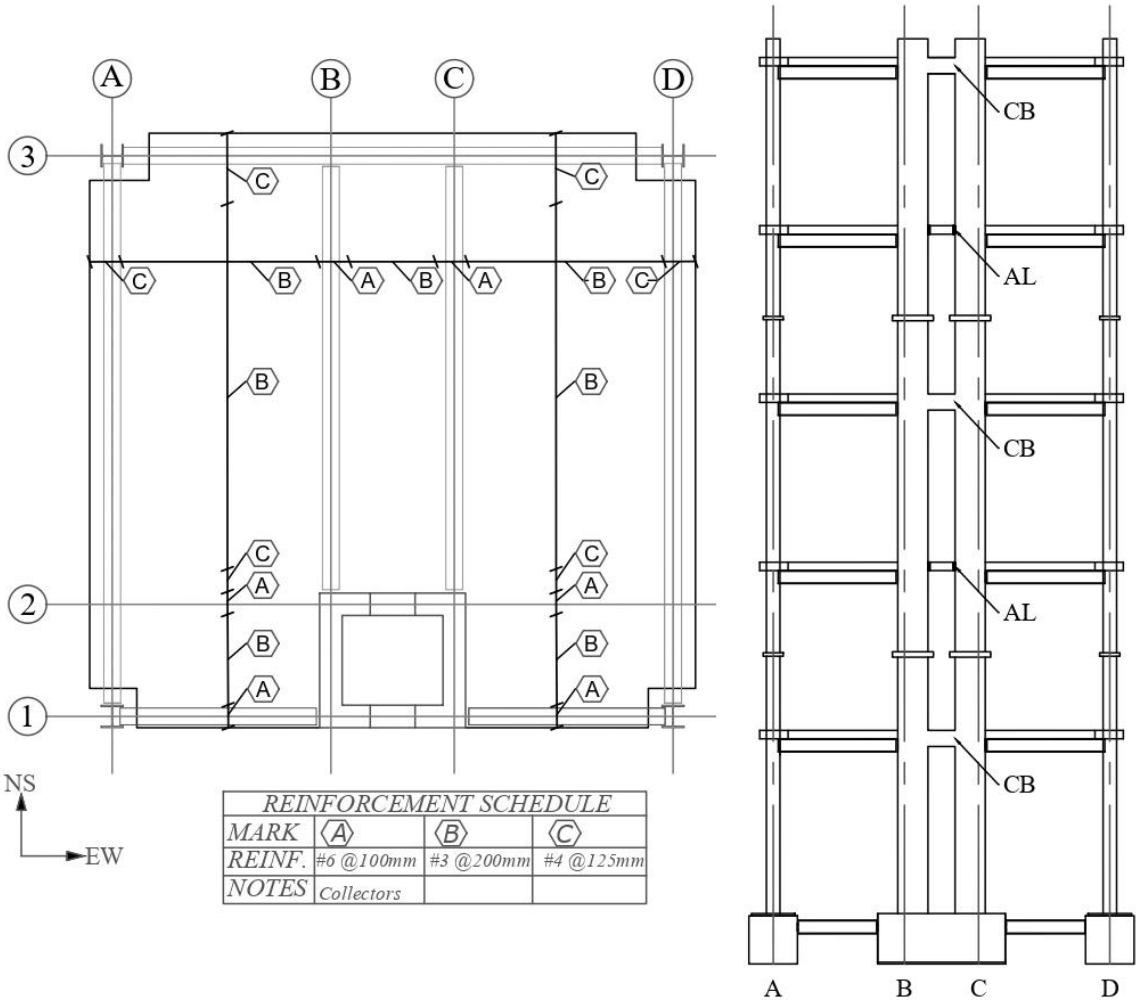
## *2.3 Structural elements*

*RC coupled wall*

The RC coupled walls consisted of two symmetric C-shaped walls connected by coupling beams (CB) at the 1st, 3rd, and 5th levels, and by pinned axial links (AL) at the 2nd and 4th levels (see Fig. 3). Each wall section had a NS length of 1200 mm, EW width of 450 mm, and a uniform thickness of 200 mm. Reinforcement details of the C-shaped walls, coupling beams, and axial links are shown in Fig. 4. Total

longitudinal reinforcement ratio for each wall was 1.6%, while longitudinal reinforcement ratio calculated in each flange of the wall section was 1.8%. For anchorage, longitudinal reinforcement was full-penetration welded to the end plates connecting adjacent modules. At the foundation, longitudinal bars of each wall extended 47 bar diameters (750 mm) below the wall-foundation interface and were welded to a steel plate located below the foundation. Volumetric reinforcement ratios calculated for the concrete within confining hoop centrelines of each wall ranged from 1% to 1.2%.

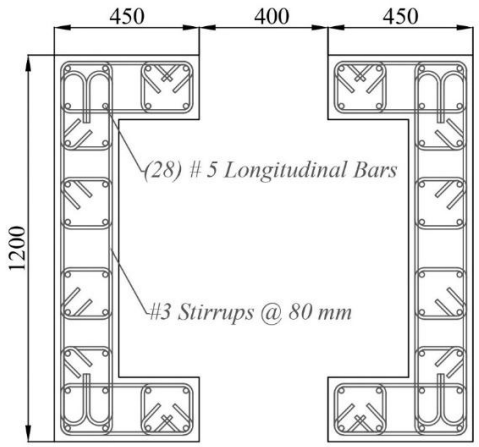
The span and depth of all coupling beams were 400 mm and 240 mm, respectively (span-to-depth ratio of 1.7). Beam width was 200 mm, matching the width of adjacent wall sections. Diagonal reinforcement consisted of two sets of intersecting bars, each consisting of four #4 (12 mm diameter) headed bars with an embedment length of 30 bar diameters (360 mm), placed at a 20-degree angle, as shown in Fig. 4(b). Horizontal and diagonal bars were confined with closed hoops and crossties with a spacing of 80 mm. Transverse reinforcement ratio provided by the stirrups was 0.7%. The coupling ratio, defined as the ratio of overturning moment resisted by coupling beams to the total overturning moment of the wall system, was 53% (El-Tawil et al., 2010; Hung & Lu, 2017). Pinned axial links were designed to tie the diaphragm together, while limiting coupling ratio, base-shear strength and overturning moment to protect testing equipment. The depth of axial links was 125 mm. 25-mm thick Styrofoam pads were provided at the interface between axial links and wall sections. Longitudinal reinforcement consisted of two #6 bars (19 mm diameter) that extended 200 mm from the external face of the wall sections as starter bars for the diaphragm reinforcement. Transverse reinforcement of axial links consisted of two plain bar spirals with a bar diameter of 6 mm and an outer diameter of 95 mm. Photographs of the reinforcement of coupling beams and coupled walls, and an elevation view of the coupled walls are shown in Fig. 5(a) and Fig.5(b), respectively.



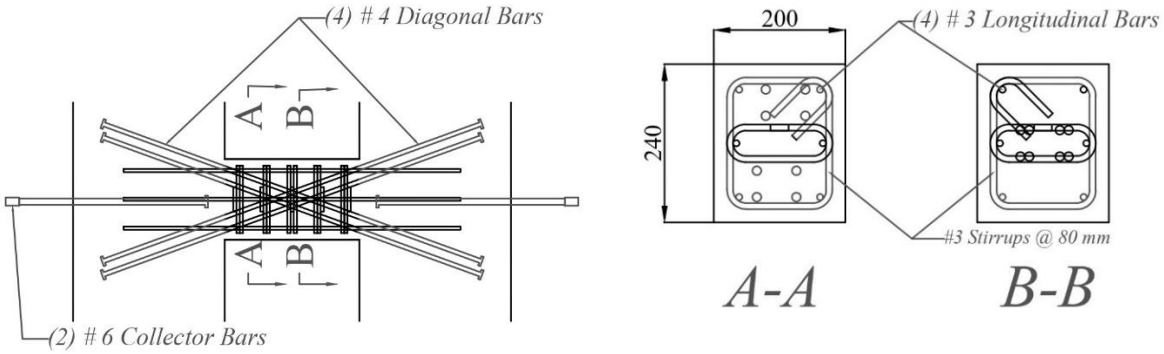

a) b)

**Fig. 3.** a) Plan view and reinforcement schedule of slabs, and b) elevation of south façade showing locations of coupling beams (CB) and axial links (AL)

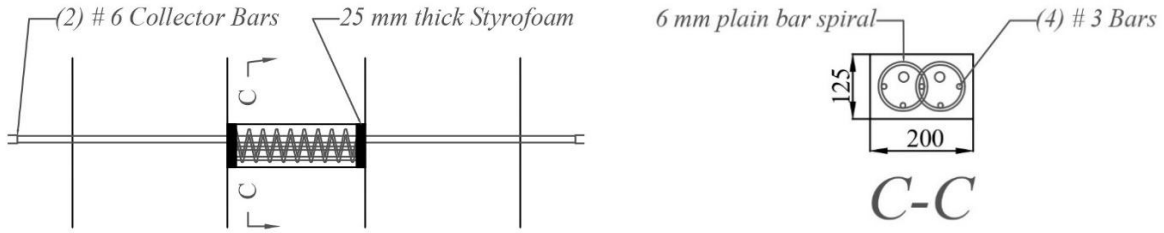
203




a)



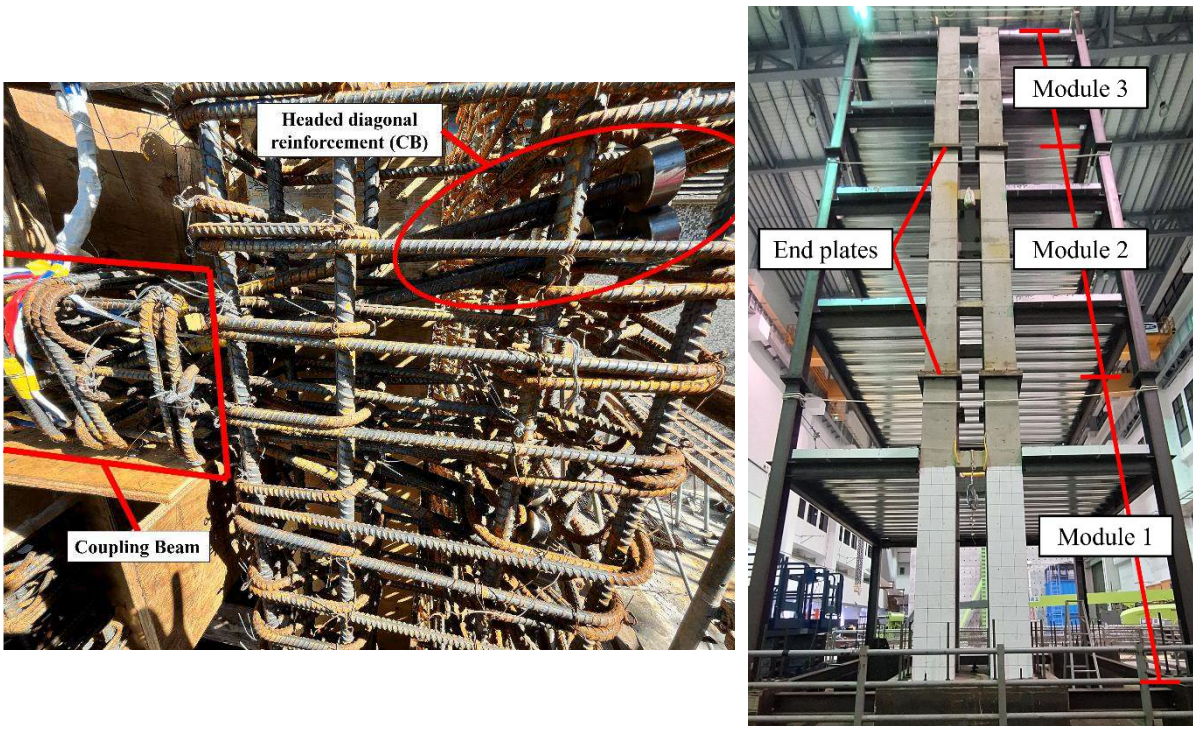

b)




c)

**Fig. 4.** Reinforcement details of (a) coupled wall, (b) coupling beams, and (c) axial links (dimensions in mm).

204




a) b)

**Fig. 5.** Photographs of a) typical reinforcement of coupling beams and coupled walls, and b) elevation view of the coupled walls.

205

206 *Composite slabs*

207

208 All floors consisted of a 125-mm thick composite slabs with a 2WH-36 trapezoidal steel decking aligned
209 with the EW direction of the building. Reinforcement details are illustrated in Fig. 3. The slab was
210 supported by perimeter beams and internal beams along gridlines B and C. Shear studs, with a diameter
211 of 16 mm, were welded to the beams with a 300 mm spacing. The first line of studs near the RC coupled
212 walls on gridlines B and C was omitted to reduce axial restraint on the coupling beams. Two #6 collector
213 bars were provided along gridlines 1, 2, B, and C, which were coupled to the starter bars embedded in
214 the wall using threaded couplers. Welded splices were used for the other reinforcing bars around the
215 wall and are shown in Fig. 6.

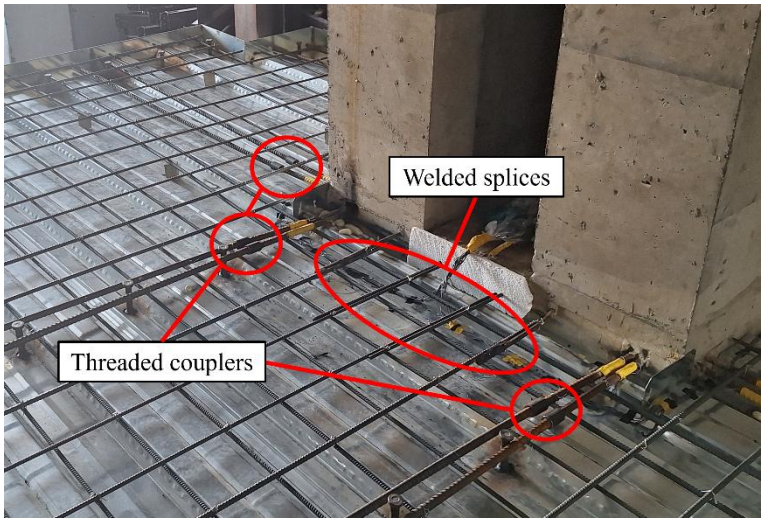



**Fig. 6.** Photograph of typical diaphragm reinforcement, showing locations of welded splices and threaded couplers.

216

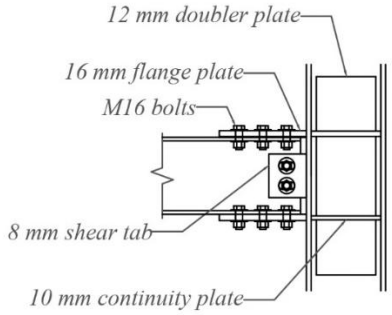
217 *Structural steel frame*

218

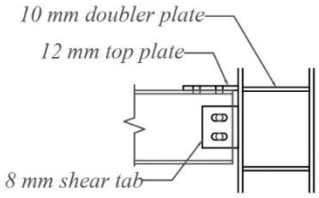
219 All steel columns had H-sections of 200×200×8×12 (outer depth × width × web thickness × flange
220 thickness), and all steel beams had H-sections of 194×150×6×9. Typical details of connections are
221 illustrated in Fig. 7. In the NS direction, all beam-column connections were detailed as pinned, as shown
222 in Fig. 7(a), with a 12-mm thick cover plate and an 8-mm thick shear tab with slotted holes. In the EW
223 direction, bolted flange-plate moment-resisting connections, as shown in Fig. 7(b), were provided at
224 joints 3A on levels 1, 3, and 5, and at joint 3D on levels 2, 4 and 5. All flange plates were 16-mm thick,

connected to the beam flanges with Grade 10.9 M16 bolts. The panel zones of the columns were reinforced with 12-mm doubler plates and 14-mm horizontal stiffeners. The plastic hinge regions of the beams along grids 3, A, B, C, and D were reinforced by 10-mm vertical stiffeners. The steel beam-RC wall connection consisted of a 10-mm thick shear tab with slotted holes, welded to a 12-mm thick plate embedded on the face of the RC wall, as shown in Fig. 7(c). For anchorage to the RC wall, 4 #3 bars (10 mm diameter) with an embedment length of 40 bar diameters (400 mm) and a Grade 10.9 M13 shear stud at the geometric centre of the face plate were full-penetration welded to the face plate. Photographs of typical connections described above are shown in Fig. 8.

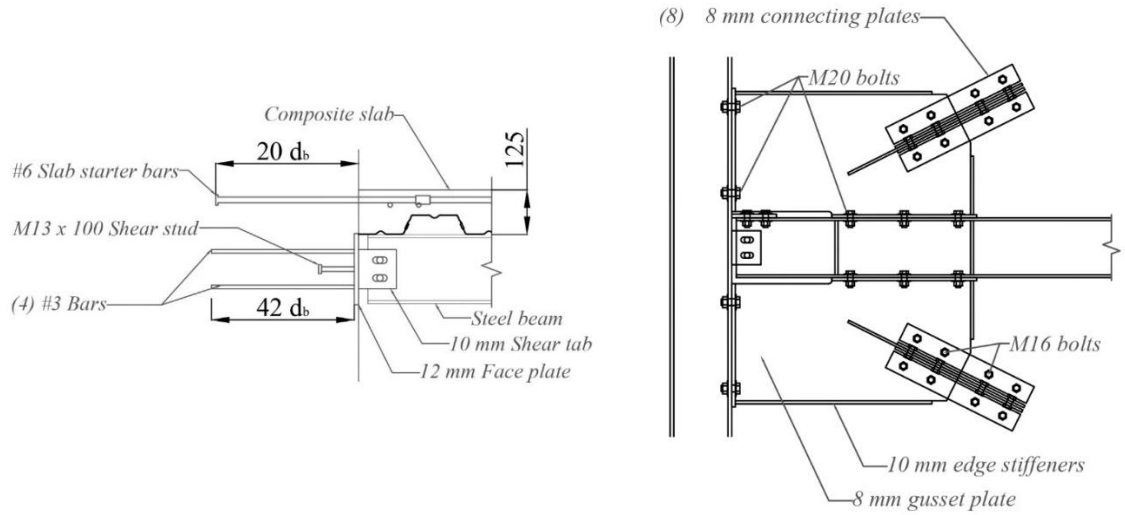
Four sandwiched buckling-restrained braces (sBRBs) with different geometries were installed on the north façade in storeys 1 to 4 before the start of the 2nd phase of the experimental program. Each sBRB was comprised of a flat steel core plate and two bolted steel restraining members. Typical top and side views of the SBRBs are shown in Figs 9(a) and 9(b), respectively. Restraining members were assembled by welding a channel section to a flat plate, as shown in Fig. 9(c). Both ends of each brace were connected to 8-mm thick gusset plates, provided with 10-mm thick edge stiffeners. Gusset plates were bolted to their corresponding steel column and beam using 10 M20 S10T bolts, as shown in Fig. 7(d).




a)




b)




c) d)

**Fig. 7.** Connections: a) moment-resisting steel beam-column connection at joint 3A in levels 1, 3, and 5, and at joint 3D in levels 2, and 4, b) pinned beam-column steel connection, c) steel beam-RC wall connection, and d) gusset plate connection

241



a) b)

c)

**Fig. 8.** Photographs of a) typical beam-column pinned connections of columns 1A and 1D, b) typical beam-column moment-resisting connection in grid 3, and d) typical braced connection.

242

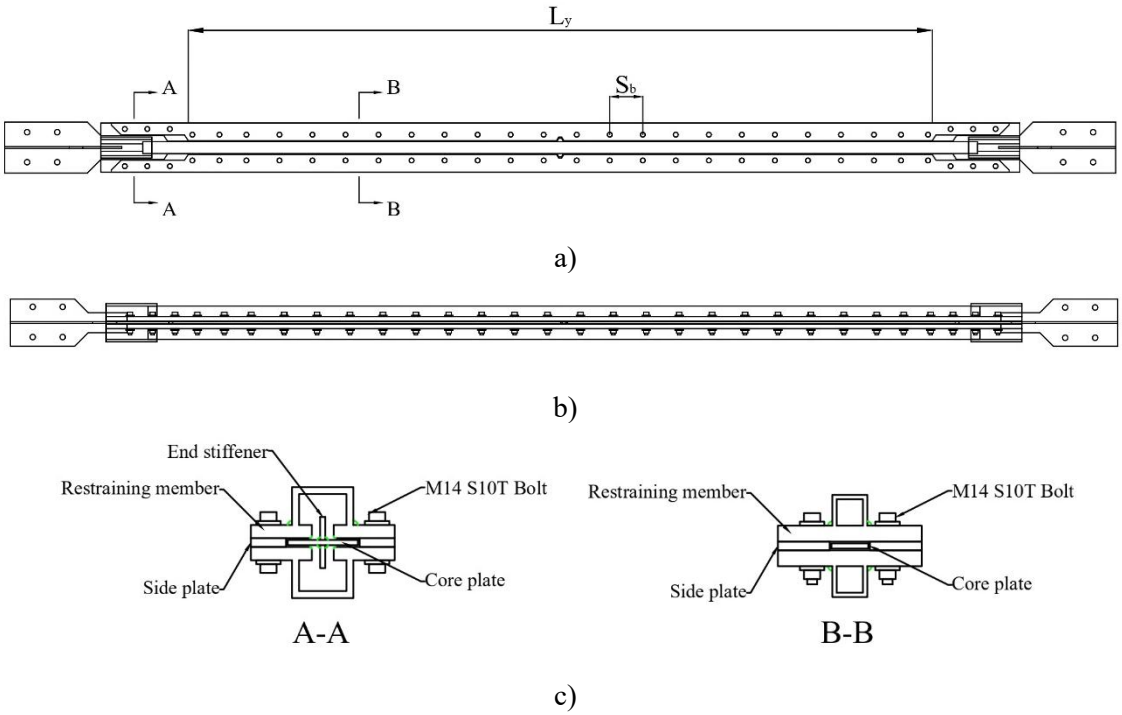



**Fig. 9.** a) Typical top view, b) side view, and c) cross section of sandwiched Buckling-Restrained Braces (sBRBs) showing the yielding length of the core plate ($L_y$) and bolt spacing of the restraining elements ($S_b$)

243

244 *Material properties*

245

246 All RC elements were constructed using a C40/50 concrete mix (nominal cylinder compressive strength
247 of 40 MPa and nominal cube compressive strength of 50 MPa) and cured under ambient conditions.
248 Standard concrete cylinder tests were performed 28 days after casting of each RC component and at
249 both the beginning and end of the experimental program, which lasted from day 60, 110, and 141 to
250 day 96, 142, and 180 after casting of the lower, middle, and upper modules, respectively. Average
251 measured 28-day compressive strength obtained from 13-cylinder tests was 35 MPa for the coupled
252 walls, coupling beams, and foundation blocks, with a coefficient of variation (COV) of 0.2. Average
253 compressive strength measured before the start of the tests obtained from 18-cylinder tests was 29 MPa
254 for the coupled walls, coupling beams, and foundation blocks, with a COV of 0.3. Average compressive
255 strength measured after the end of the tests obtained from 15-cylinder tests was 34 MPa for the coupled
256 walls, coupling beams, and foundation blocks. For the composite slabs, the average measured 28-day
257 compressive strength obtained from a total of 9-cylinder tests was 24 MPa, with a COV of 0.1. Three

#3, #4, #5, and #6 reinforcing bars each were tested in tension. The average measured yield stresses were 464, 476, 442, and 459 MPa, respectively, and the corresponding average ultimate stresses were 685, 684, 642, and 659 MPa. All structural steel elements used SS400A steel, with nominal yield and ultimate stresses of 205 MPa and 400 MPa, respectively.

### *2.4 Non-structural elements*

The non-structural elements installed in the 2nd and 3rd stories formed two rooms separated by a corridor (Fig. 10). The partition walls of each room had different head and base track connections, as well as different corner detailing. The detailing of the rooms on the west side of the building in both stories was identical and representative of conventional partition walls in New Zealand. The only difference was that the room on the 3rd story was fire-rated, which means plasterboard lining spanned full-height, and the gap between the lining and the soffit was filled with fire-rated sealant. The rooms on the east side of the building were built using alternatives expected to incur less damage. As shown in Fig. 11(a), the east room on the 2nd story had a flexible top bracket to de-couple walls from the top slab, while in the east room on the 3rd story, studs were not screwed to both the base and head tracks to allow relative displacements between partition walls and floors. 20 mm gaps filled with sealant were provided at the edge of each partition wall to accommodate interactions between partitions, as illustrated in Fig. 11(b).

Concealed ceilings were installed inside each room on the 2nd and 3rd stories using fixed connections around their perimeter, while fully floating ceilings were installed for the corridor, as shown in Fig. 10. All ceilings had two layers of plasterboard and thus increased mass to compensate for their reduced areas. A sprinkler pipe system was installed on the plenum of the 3rd story rooms. Flexible and rigid penetration details were used for penetration joints through partition walls. Branch pipes terminated with sprinkler heads that penetrated through the concealed ceilings into each room were also installed. The east room on the 2nd story was filled with day-to-day appliances, including a desktop computer, two office chairs, and two small bookshelves.

The 4th story had four T-shaped partition walls with detailing practices typical from Taiwan. Top and base connections of the partitions were fixed and a 10 mm gap at the top of the plasterboard was reserved and remained unsealed. Veneer panels of different thicknesses were attached to the partition walls. On the 5th story, two identical library shelves were installed, each of which was loaded with approximately 500 kg of books. A photograph of the non-structural components included in the tests is shown in Fig. 12.

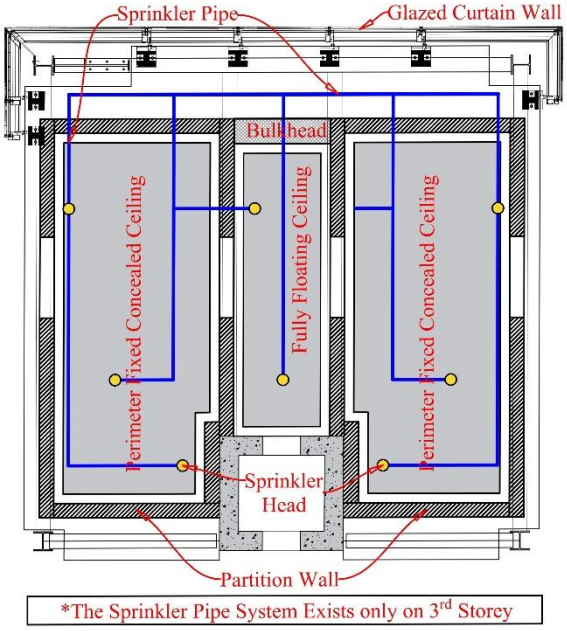



**Fig. 10.** Plan view of NSC installed on 2nd and 3rd stories.

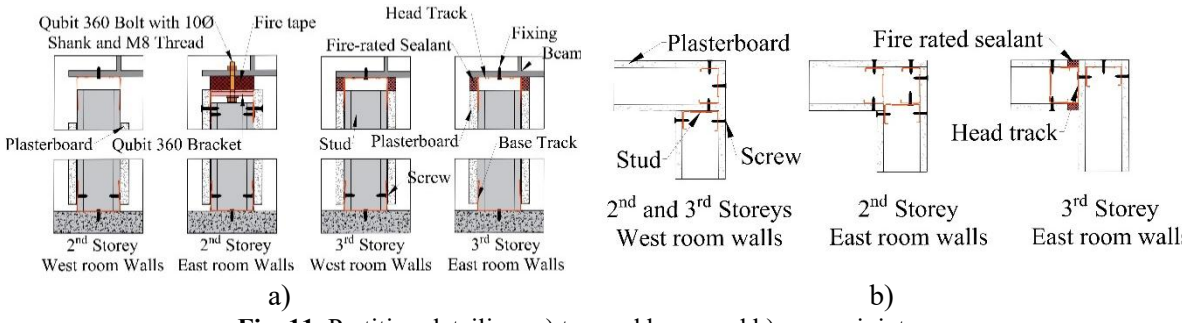



**Fig. 11.** Partition detailing: a) top and base, and b) corner joints.

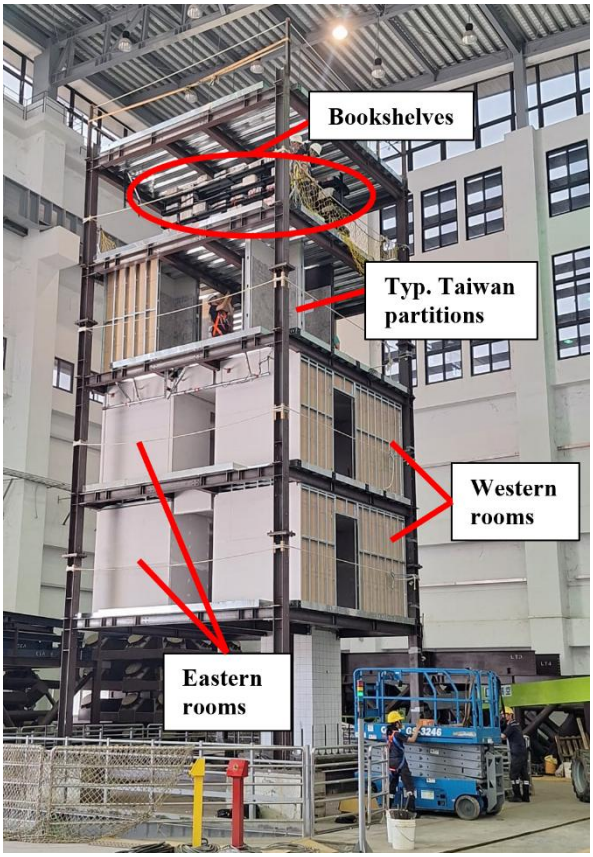



**Fig. 12.** Photograph showing the location of the non-structural components included in the building specimen.

295

## 296 3. Experimental program

297

### 298 *3.1 Test sequence*

299

300 A total of 42 earthquake motions were simulated using the high-performance triaxial earthquake
301 simulator in the National Center for Research on Earthquake Engineering (NCREE) Laboratory in
302 Tainan, Taiwan. Original ground motion records were scaled to match the design spectrum of the
303 building for a range of periods of interest (0.4 s. to 1.0 s.). The 'design intensity' corresponded roughly
304 to a ground motion with a PGV of 40 cm/s, a PGA of 0.4 g, and a displacement spectrum reaching 200
305 mm for a period of 1 s and a damping ratio of 2%. Applied ground motions were selected based on two
306 factors: 1) scaled peak ground acceleration, velocity, and displacements had to remain within the limits
307 of the equipment, and 2) the spectral displacement had to increase with period as linearly as possible
308 inside the range of periods of interest. Based on these criteria, the ground motion recorded during the

1940 El Centro, California earthquake was selected for the majority of excitations. Target PGV of the applied ground motions was further scaled to represent different intensities, as reported in Table 2. Fig. 9 shows the reference design spectrum and the elastic spectra of El Centro (1940) ground motions scaled to a PGV of 40 cm/s and a damping ratio of 5%. Three additional ground motions recorded during the 1999 Chi-Chi, Taiwan earthquake (CHY006), the 1995 Kobe, Japan earthquake (JMA), and the 2011 Christchurch, New Zealand earthquake (RE.HS.) were also included in Phase 3 of the experimental program for two tests each. The additional motions were scaled as indicated by the measures listed in Table 2.

The tests were conducted in 3 phases. The unbraced building configuration was used in phase 1, where 8 simulated earthquake excitations (i.e. test runs) with relatively low intensities (measured PGV between 8 cm/s and 26 cm/s) were performed. Phase 2 consisted of 16 simulated earthquake excitations using the braced configuration. After removal of braces and installation of a curtain wall on the north façade, 18 test runs were performed in Phase 3 using the unbraced building configuration. Peak ground parameters of each test run are summarized in Table 2. Before and after each test run, the building was subjected to three-directional white noise excitations with a PGA of approximately 0.03 g.

**Table 2.** Test matrix.

| Run | Record | Direction [a] | Config. | NS | | | EW | | |
|---|---|---|---|---|---|---|---|---|---|
| | | | | PGA [g] | PGV [cm/s] | PGD [mm] | PGA [g] | PGV [cm/s] | PGD [mm] |
| - | Table Limits | - | - | ±1.4 | ±200 | ±1000 | ±1.4 | ±200 | ±1000 |
| 1 | El Centro 1940 | X | Unbraced | - | - | - | 0.08 | 10 | 36 |
| 2 | El Centro 1940 | Z | | 0.16 | 13 | 31 | - | - | - |
| 3 | El Centro 1940 | X+Z | | 0.15 | 13 | 33 | 0.09 | 10 | 36 |
| 4 | El Centro 1940 | X+Y+Z | | 0.16 | 13 | 32 | 0.09 | 10 | 35 |
| 5 | El Centro 1940 | X | | - | - | - | 0.17 | 20 | 70 |
| 6 | El Centro 1940 | Z | | 0.34 | 25 | 63 | - | - | - |
| 7 | El Centro 1940 | X+Z | | 0.34 | 26 | 68 | 0.19 | 20 | 69 |
| 8 | El Centro 1940 | X+Y+Z | | 0.36 | 26 | 63 | 0.17 | 20 | 74 |
| 9 | El Centro 1940 | X | Braced | - | - | - | 0.07 | 9 | 31 |
| 10 | El Centro 1940 | Z | | 0.15 | 14 | 24 | - | - | - |
| 11 | El Centro 1940 | X+Z | | 0.15 | 14 | 25 | 0.09 | 9 | 30 |
| 12 | El Centro 1940 | X+Y+Z | | 0.15 | 15 | 29 | 0.09 | 9 | 32 |
| 13 | El Centro 1940 | X | | - | - | - | 0.17 | 18 | 65 |
| 14 | El Centro 1940 | Z | | 0.31 | 28 | 49 | - | - | - |

| | | | | | | | | | |
|---|---|---|---|---|---|---|---|---|---|
| 15 | El Centro 1940 | X+Z | | 0.31 | 30 | 58 | 0.18 | 19 | 68 |
| 16 | El Centro 1940 | X+Y+Z | | 0.32 | 30 | 59 | 0.20 | 20 | 70 |
| 17 | El Centro 1940 | X+Z | | 0.31 | 30 | 55 | 0.19 | 19 | 70 |
| 18 | El Centro 1940 | X+Y+Z | | 0.31 | 30 | 54 | 0.20 | 19 | 60 |
| 19 | El Centro 1940 | X+Y+Z | | 0.44 | 44 | 77 | 0.31 | 28 | 98 |
| 20 | El Centro 1940 | X+Z | | 0.60 | 60 | 109 | 0.41 | 39 | 125 |
| 21 | El Centro 1940 | X+Y+Z | | 0.59 | 62 | 101 | 0.44 | 40 | 136 |
| 22 | El Centro 1940 | X+Z | | 0.73 | 74 | 128 | 0.52 | 52 | 166 |
| 23 | El Centro 1940[b] | X+Z | | 0.55 | 51 | 155 | 0.70 | 70 | 152 |
| 24 | El Centro 1940[b] | X+Z | | 0.66 | 61 | 203 | 0.84 | 84 | 176 |
| 25 | El Centro 1940 | X+Y+Z | | 0.16 | 16 | 28 | 0.11 | 11 | 33 |
| 26 | El Centro 1940 | X+Y+Z | | 0.15 | 15 | 26 | 0.09 | 11 | 33 |
| 27 | El Centro 1940 | X+Y+Z | | 0.30 | 29 | 49 | 0.21 | 20 | 67 |
| 28 | El Centro 1940 | X+Y+Z | | 0.41 | 46 | 84 | 0.29 | 32 | 106 |
| 29 | El Centro 1940 | X+Y+Z | | 0.53 | 58 | 99 | 0.39 | 43 | 125 |
| 30 | El Centro 1940 | X+Z | | 0.66 | 74 | 139 | 0.48 | 55 | 177 |
| 31 | El Centro 1940 [b] | X+Z | | 0.49 | 54 | 160 | 0.73 | 82 | 153 |
| 32 | El Centro 1940 | X+Y+Z | | 0.31 | 30 | 52 | 0.20 | 23 | 66 |
| 33 | El Centro 1940 | X+Y+Z | Unbraced | 0.43 | 46 | 80 | 0.30 | 35 | 105 |
| 34 | El Centro 1940 [b] | X+Z | | 0.49 | 57 | 144 | 0.73 | 75 | 135 |
| 35 | Chi-Chi 1999 | X+Y+Z | | 0.37 | 43 | 85 | 0.42 | 59 | 162 |
| 36 | Kobe (1995) | X+Y+Z | | 0.41 | 45 | 79 | 0.32 | 37 | 83 |
| 37 | Christchurch 2011 | X+Y+Z | | 0.22 | 24 | 60 | 0.35 | 39 | 136 |
| 38 | El Centro 1940 [b] | X+Z | | 0.60 | 65 | 192 | 0.89 | 97 | 185 |
| 39 | Chi-Chi 1999 | X+Y+Z | | 0.19 | 24 | 48 | 0.20 | 30 | 83 |
| 40 | Kobe (1995) | X+Y+Z | | 0.20 | 23 | 43 | 0.16 | 21 | 43 |
| 41 | Christchurch 2011 | X+Y+Z | | 0.11 | 12 | 31 | 0.18 | 19 | 57 |
| 42 | El Centro 1940 [b] | X+Z | | 0.60 | 67 | 181 | 0.89 | 94 | 160 |

[a] X: NS direction (+X is south); Z: EW direction (+Z is east); Y: vertical direction (+Y is up)

[b] NS and EW components swapped

Note: NS components of the ground motion records were applied in the NS direction of the specimen, unless otherwise noted.

327

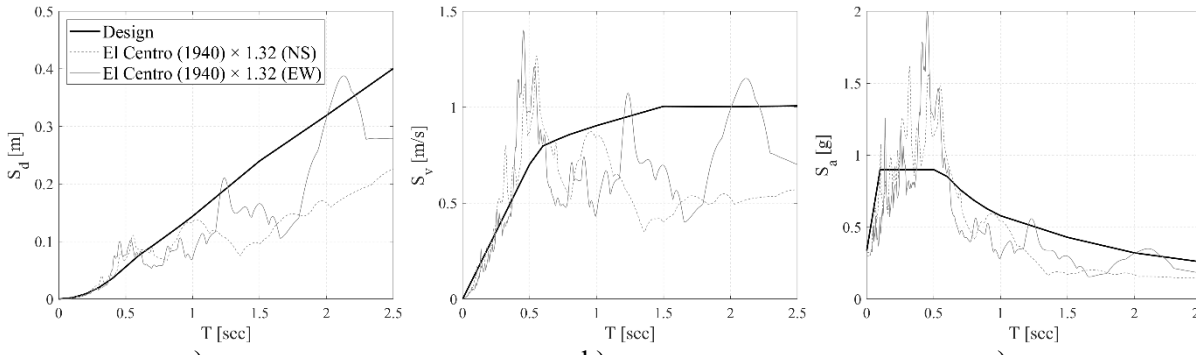



**Fig. 9** Design and calculated a) displacement spectrum ($S_d$), b) velocity spectrum ($S_v$), and c) acceleration spectrum ($S_a$) with a damping ratio of 5% for test runs reaching approximately a PGV of 40 cm/s in each direction.

328

### *3.2 Instrumentation*

Sensors monitored both the global response of the test specimen and local performance of all structural and non-structural elements. Figs. 13 and 14 show the location of key sensors. To monitor the applied excitations, three triaxial accelerometers were installed on the platform of the earthquake simulator, located at the projected centre of mass of the structure and near the north-east and south-west floorplan corners. To measure floor accelerations during each excitation, two triaxial accelerometers were installed on each floor of the structure, located at the centre of mass and north-east corner. An array of over 350 motion capture targets was installed to capture displacements and element deformations. Story drift on the north façade was also measured using eight cameras installed on each floor. The cameras tracked the relative displacements and rotations of an LED target installed on the floor above.

Horizontal slip of each foundation block was monitored by two displacement transducers, while the uplift of each foundation block was monitored by two additional displacement transducers located at opposite corners of the foundation blocks for the north-west and south-east columns and RC coupled walls. Vertical, horizontal, and diagonal deformations near the base of the RC coupled wall were measured using electromagnetic transducers installed on the north and east wall faces. Strain gauges were installed on longitudinal and transverse reinforcement of the coupled wall and coupling beams, and at critical sections of gusset plates, sBRBs, and steel columns. Additional details are available upon request.

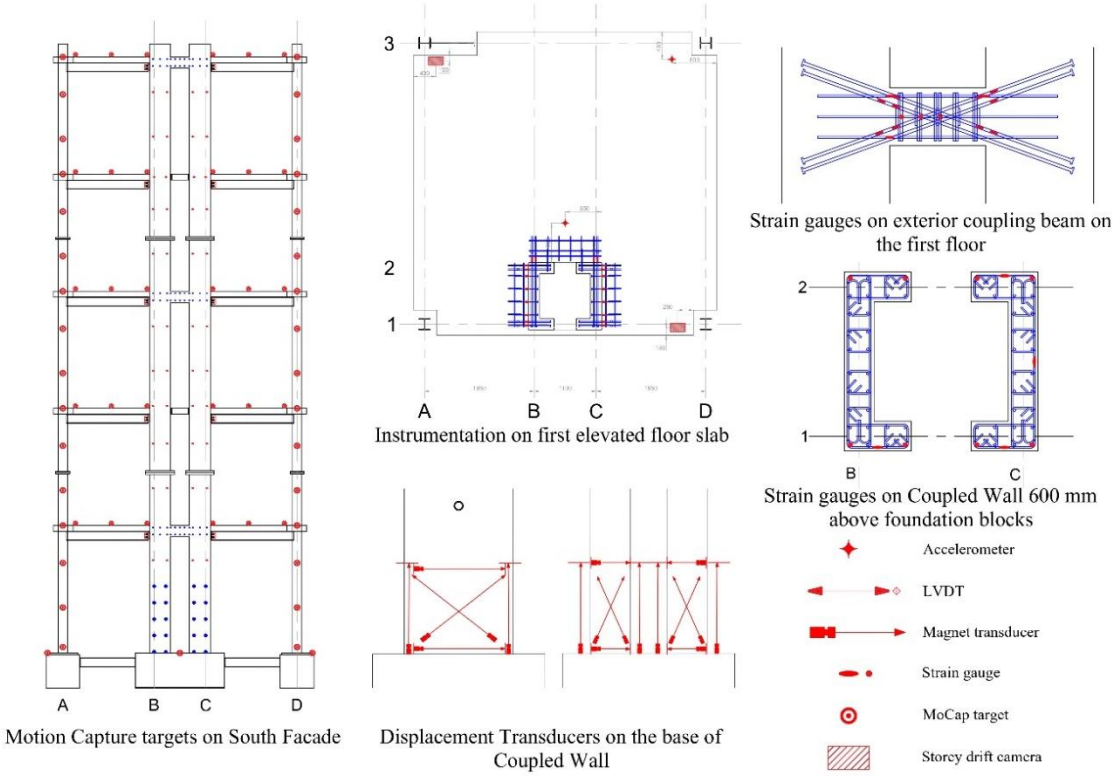
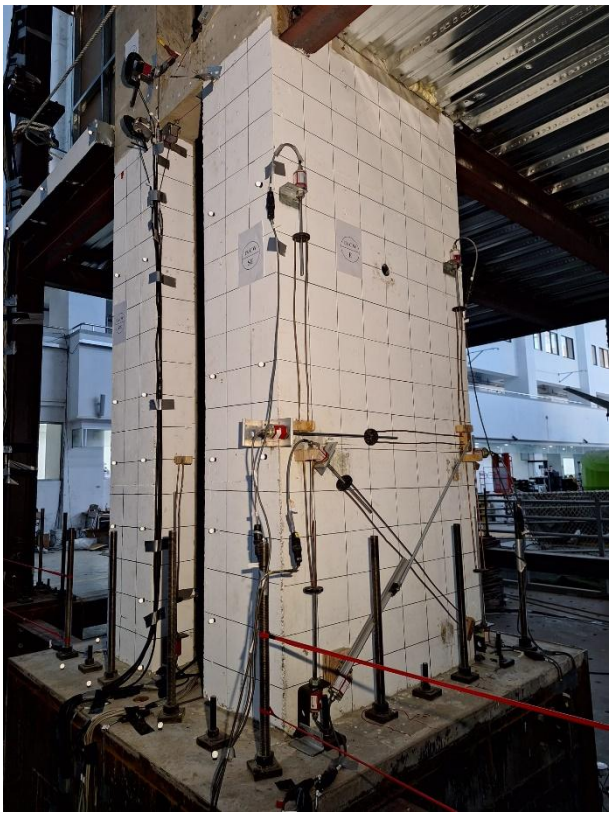



**Fig. 13.** Location of key sensors

350



a)




b)

**Fig. 14.** Photographs of a) instrumentation installed on the coupled walls in the first storey, and b) motion capture sensors installed on the coupling beam at the fifth floor.

351

352 ## 4. Test results

353

354 ### *4.1 Global building response*

355

356 Table 3 summarizes the overall building responses for all 42 simulated earthquake motions.
357 Accelerations records were filtered to exclude frequencies outside the range of 0.125-40 Hz before
358 integration to obtain velocities and displacements. Roof-drift ratios (RDR) and storey-drift ratios (SDR)
359 were calculated based on displacement records measured by the motion capture system and confirmed
360 using data from the accelerometers installed on each floor. In the EW direction, RDR and SDR for the
361 south façade (SF), centre of mass (CoM), and north façade (NF) are reported in Table 3. In the NS
362 direction, only RDR and SDR at CoM are presented for brevity. Deflected shapes measured at peak
363 roof-drift at the centre of mass are illustrated in Fig. 15. The overall deflected shape at the CoM seemed
364 to stay constant as the amplitude of deflections increased.

365

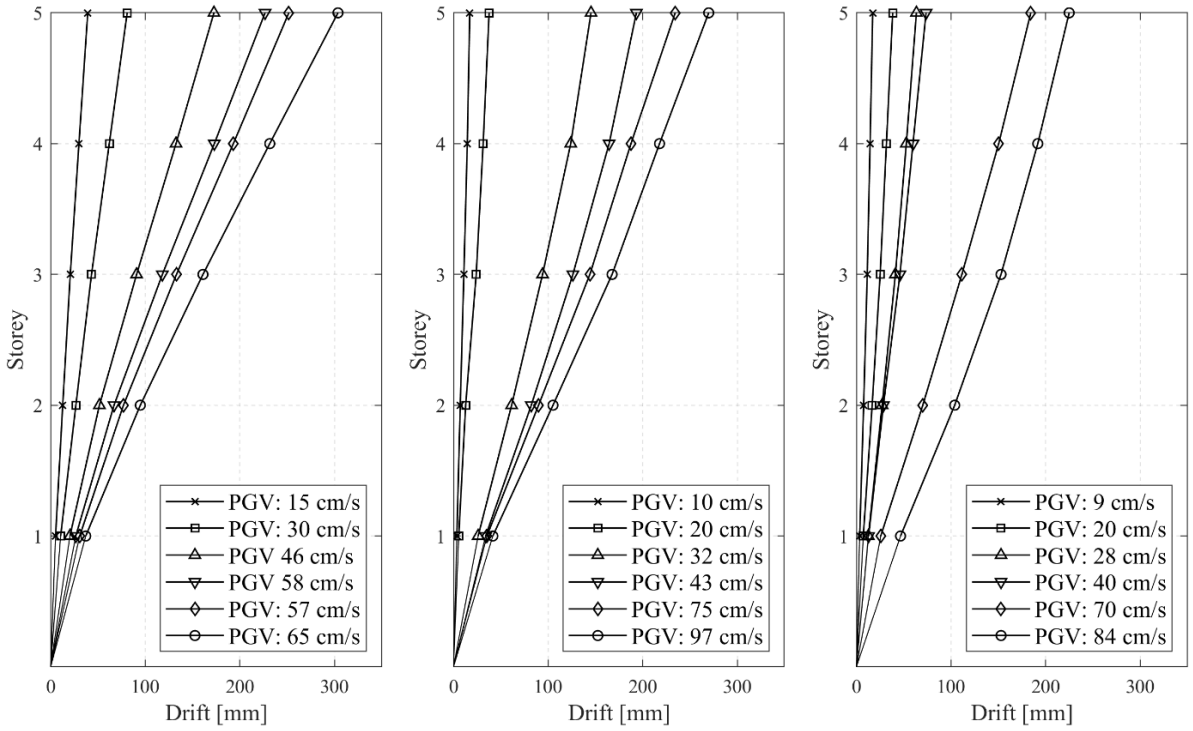



**Fig. 15.** Deflected shapes measured at centre of mass in a) NS direction, b) EW direction for unbraced configuration, and c) EW direction for braced configuration.

366

367 Maximum RDR and SDR at the CoM increased in nearly proportional fashion to PGV for the building
368 configurations tested, as shown in Fig. 16. Outliers were observed when the ground motion records
369 from 1999 Chi-Chi earthquake and 2011 Christchurch earthquake were used. For these tests, the rate of
370 increase of drift was also proportional to PGV, with the main difference being that larger drift demands
371 were measured for test runs with the same PGV compared to tests using the El Centro ground motion
372 record. This observation suggests that drift demands were sensitive to the shape of the displacement
373 spectrum of a given ground motion.

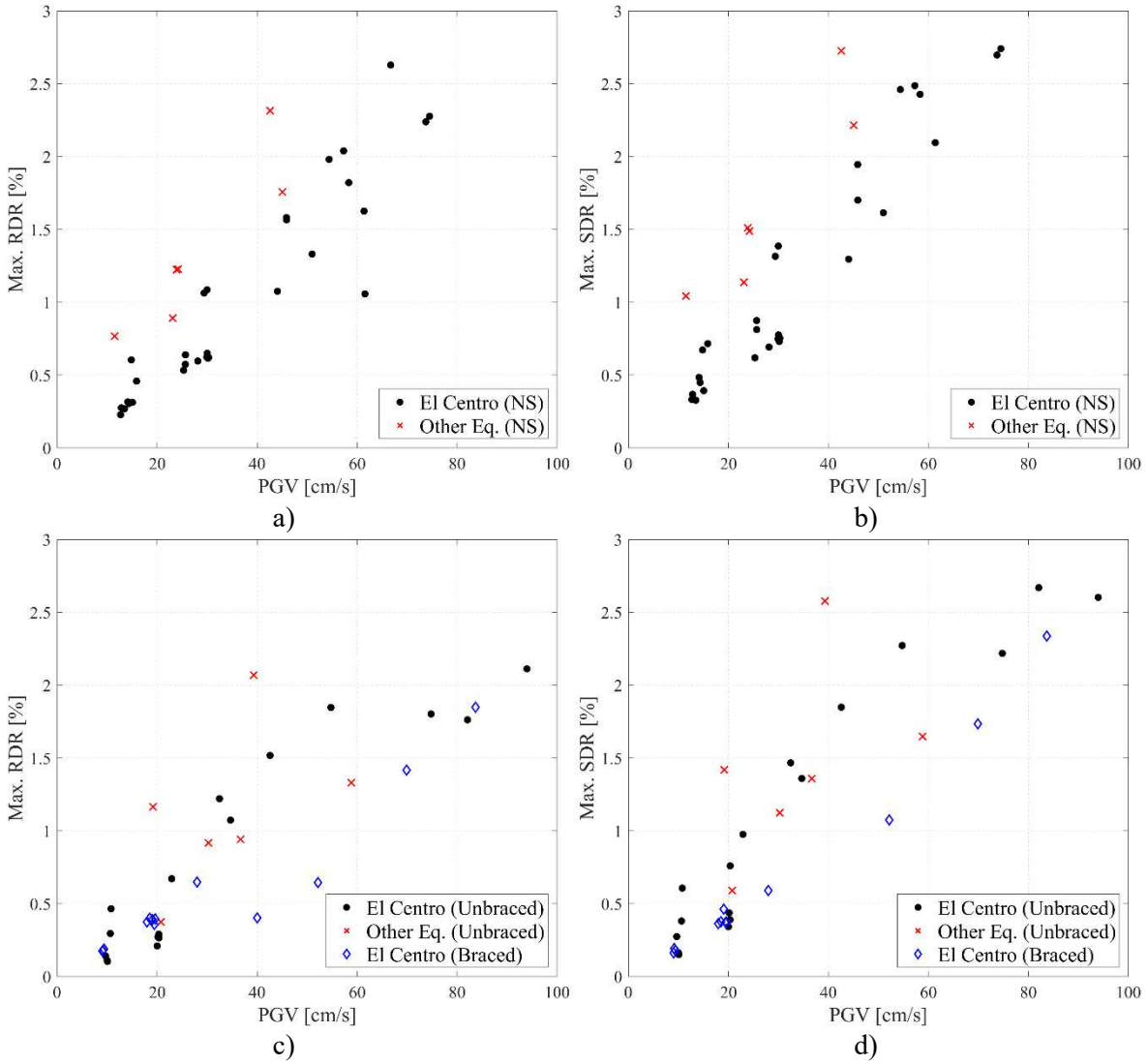



**Fig. 16.** Drift ratio vs. PGV: a) maximum RDR in NS direction, b) maximum SDR in NS direction, c) maximum RDR in EW direction, and d) maximum SDR in EW direction.

374

375 For repeats of the same ground motion and for a given building configuration, e.g., run 4 (initial run)
376 vs. run 25 (repeated run), RDR and SDR were on average 40% larger than those from initial runs. If
377 runs in which SDR did not surpass 0.5% are excluded (representing possible instances in which no
378 cracking and/or yielding occurred in the RC elements during the initial run), drift ratios measured on
379 repeated runs were on average 10% larger than those measured in initial runs. Decreases in stiffness
380 (represented by period elongations as the tests progressed), seemed to occur simultaneously with
381 increases in damping, resulting in comparable drift demands during repeated and initial runs.

382

Maximum floor displacements measured at the centre of mass, maximum base shear, and maximum base moment were observed to occur nearly simultaneously for each test run. Instances in which maximum displacements were observed in one direction were usually accompanied by near-zero displacements in the perpendicular direction. These observations suggest that maximum floor displacements at the centre of mass were dominated by the fundamental mode of the structure in each direction.

The façade in which maximum RDR and SDR were recorded in the EW direction varied with building configuration and displacement history. Changes in the deflected shape due to torsional effects were quantified using the ratio of floor displacements in the North façade to floor displacements in the South façade for levels 1, 3, and 5. As shown in Fig. 17, floor displacement ratios gradually decreased during Phase 1 as a consequence of cracking in the RC wall in the South façade, while no yielding of the steel columns or cracking of the composite slab near the North façade was observed. During phase 2, ratios of floor displacements were nearly constant. Maximum RDR and SDR in Phase 2 were 2.4% and 2.9%, respectively. Those values were recorded in the South façade during test run 24. During Phase 3, the ratio of floor displacements in the North and South façades increased as cracking of the composite slab extended to the North façade and steel columns yielded. It is worth noting that the ratio was smaller than 1 before test run 30, which means larger floor displacements were observed in the south façade, even after the removal of sBRBs. Maximum RDR and SDR in Phase 3 were 2.3% and 3.7%, respectively. Those values were recorded in the north façade during the test run 42.

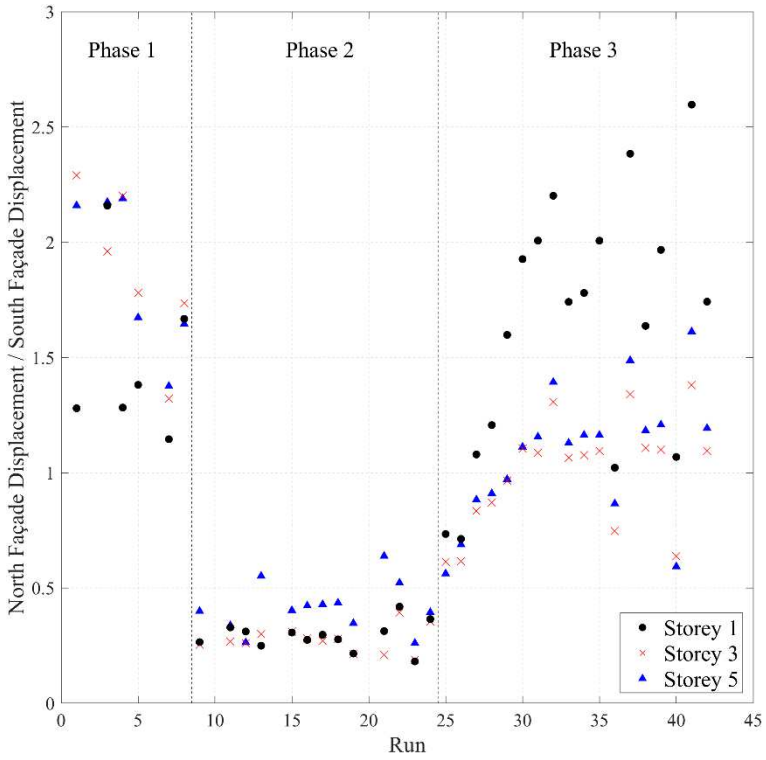



**Fig. 17.** Ratio of north to south façade floor displacements.

404

405 **Table 3.** Summary of global response.

| Configuration | Run | NS Direction | | | | EW Direction | | | | | | | |
|---|---|---|---|---|---|---|---|---|---|---|---|---|---|
| | | RDR CoM [%] | SDR[a] CoM [%] | $V_b$ [kN] | $M_b$ [kN.m] | RDR NF [%] | SDR[a] NF [%] | RDR CoM [%] | SDR[a] CoM [%] | RDR SF [%] | SDR[a] SF [%] | $V_b$ [kN] | $M_b$ [kN.m] |
| Unbraced | 1 | - | - | - | - | 0.2 | 0.3 (3) | 0.1 | 0.2 (2) | 0.1 | 0.1 (2) | 67 | 527 |
| | 2 | 0.2 | 0.3 (5) | 10 | 1096 | - | - | - | - | - | - | - | - |
| | 3 | 0.3 | 0.3 (5) | 139 | 1153 | 0.2 | 0.3 (4) | 0.1 | 0.2 (4) | 0.1 | 0.1 (4) | 69 | 546 |
| | 4 | 0.3 | 0.4 (5) | 136 | 1150 | 0.2 | 0.4 (3) | 0.1 | 0.3 (4) | 0.1 | 0.2 (2) | 75 | 608 |
| | 5 | - | - | - | - | 0.4 | 0.6 (3) | 0.2 | 0.3 (2) | 0.2 | 0.3 (2) | 136 | 1110 |
| | 6 | 0.5 | 0.6 (5) | 229 | 1776 | - | - | - | - | - | - | - | - |
| | 7 | 0.6 | 0.9 (3) | 203 | 1750 | 0.4 | 0.6 (3) | 0.3 | 0.4 (4) | 0.3 | 0.4 (2) | 137 | 984 |
| | 8 | 0.6 | 0.8 (4) | 212 | 1826 | 0.4 | 0.6 (3) | 0.3 | 0.4 (2) | 0.2 | 0.3 (2) | 121 | 854 |
| Braced | 9 | - | - | - | - | 0.1 | 0.1 (4) | 0.2 | 0.2 (2) | 0.2 | 0.2 (3) | 78 | 551 |
| | 10 | 0.3 | 0.4 (3) | 90 | 710 | - | - | - | - | - | - | - | - |
| | 11 | 0.3 | 0.5 (3) | 91 | 714 | 0.1 | 0.1 (4) | 0.2 | 0.2 (3) | 0.2 | 0.2 (3) | 79 | 693 |
| | 12 | 0.3 | 0.4 (3) | 91 | 706 | 0.0 | 0.1 (4) | 0.2 | 0.2 (2) | 0.2 | 0.3 (3) | 78 | 565 |
| | 13 | - | - | - | - | 0.2 | 0.2 (4) | 0.4 | 0.4 (2) | 0.4 | 0.5 (2) | 152 | 1347 |
| | 14 | 0.6 | 0.7 (5) | 198 | 1563 | - | - | - | - | - | - | - | - |
| | 15 | 0.6 | 0.7 (3) | 201 | 1595 | 0.1 | 0.2 (3) | 0.4 | 0.4 (2) | 0.4 | 0.5 (3) | 155 | 1369 |
| | 16 | 0.6 | 0.8 (3) | 200 | 1582 | 0.2 | 0.2 (3) | 0.4 | 0.4 (2) | 0.4 | 0.5 (3) | 153 | 1368 |
| | 17 | 0.6 | 0.7 (3) | 198 | 1573 | 0.2 | 0.2 (2) | 0.4 | 0.4 (2) | 0.4 | 0.5 (5) | 149 | 1325 |
| | 18 | 0.7 | 0.8 (4) | 200 | 1582 | 0.2 | 0.2 (2) | 0.4 | 0.5 (3) | 0.4 | 0.6 (5) | 143 | 1306 |
| | 19 | 1.1 | 1.3 (4) | 297 | 2349 | 0.2 | 0.4 (2) | 0.6 | 0.6 (2) | 0.7 | 1.0 (5) | 217 | 1915 |
| | 20 [b] | 1.8 | 1.8 (3) | 282 | 3202 | 0.4 | 0.7 (2) | 0.6 | 0.6 (3) | N/A | N/A | 282 | 2228 |
| | 21 [b] | 1.9 | 2.2 (5) | 479 | 3850 | 0.4 | 0.7 (3) | 0.6 | 0.5 (3) | N/A | N/A | 292 | 2224 |
| | 22 | 2.3 | 2.7 (4) | 465 | 3625 | 0.4 | 0.9 (5) | 0.6 | 1.1 (5) | 0.8 | 1.4 (2) | 335 | 2433 |
| | 23 | 1.3 | 1.6 (3) | 594 | 2230 | 0.5 | 0.9 (2) | 1.4 | 1.7 (2) | 1.9 | 2.4 (3) | 431 | 3220 |
| | 24 | 1.6 | 2.1 (4) | 341 | 2546 | 0.9 | 1.3 (2) | 1.8 | 2.3 (2) | 2.4 | 2.9 (2) | 515 | 4171 |
| Unbraced | 25 | 0.5 | 0.7 (5) | 82 | 698 | 0.2 | 0.4 (5) | 0.3 | 0.4 (4) | 0.4 | 0.5 (2) | 62 | 437 |
| | 26 | 0.6 | 0.7 (4) | 92 | 783 | 0.2 | 0.3 (5) | 0.5 | 0.6 (2) | 0.3 | 0.5 (2) | 74 | 510 |
| | 27 | 1.1 | 1.3 (4) | 201 | 1601 | 0.2 | 0.8 (3) | 0.3 | 0.8 (4) | 0.3 | 1.0 (2) | 152 | 1142 |
| | 28 | 1.6 | 1.7 (4) | 298 | 2318 | 1.0 | 1.3 (1) | 1.2 | 1.5 (3) | 1.2 | 1.5 (2) | 236 | 1845 |
| | 29 | 1.8 | 2.4 (4) | 387 | 2992 | 1.5 | 2.0 (1) | 1.5 | 1.8 (3) | 1.5 | 1.9 (2) | 321 | 2528 |
| | 30 | 2.2 | 2.7 (5) | 441 | 3328 | 2.0 | 2.7 (1) | 1.8 | 2.3 (3) | 1.8 | 2.2 (3) | 363 | 2963 |

| | | | | | | | | | | | | |
|---|---|---|---|---|---|---|---|---|---|---|---|---|
| 31 | 2.0 | 2.5 (4) | 374 | 3044 | 1.9 | 3.0 (1) | 1.8 | 2.7 (4) | 1.6 | 2.1 (3) | 334 | 2571 |
| 32 | 1.1 | 1.4 (4) | 180 | 1219 | 0.8 | 1.1 (4) | 0.7 | 1.0 (4) | 0.6 | 0.7 (3) | 106 | 707 |
| 33 | 1.6 | 1.9 (5) | 259 | 2224 | 1.2 | 1.7 (4) | 1.1 | 1.4 (3) | 1.0 | 1.4 (3) | 162 | 1082 |
| 34 | 2.0 | 2.5 (5) | 384 | 3118 | 2.0 | 3.2 (1) | 1.8 | 2.2 (3) | 1.7 | 2.1 (2) | 337 | 1832 |
| 35 | 2.3 | 2.7 (5) | 389 | 3450 | 1.4 | 2.0 (1) | 1.3 | 1.6 (3) | 1.2 | 1.6 (3) | 201 | 1174 |
| 36 | 1.8 | 2.2 (5) | 275 | 2268 | 0.9 | 1.7 (4) | 0.9 | 1.4 (3) | 1.0 | 1.3 (3) | 127 | 884 |
| 37 | 1.2 | 1.5 (5) | 217 | 1702 | 2.6 | 3.5 (1) | 2.1 | 2.6 (3) | 1.7 | 2.2 (3) | 336 | 2610 |
| 38 | 2.5 | 3.0 (4) | 440 | 3578 | 2.3 | 3.4 (1) | 2.1 | 2.5 (3) | 1.9 | 2.4 (3) | 367 | 2813 |
| 39 | 1.2 | 1.5 (5) | 191 | 1679 | 1.0 | 1.6 (1) | 0.9 | 1.1 (3) | 0.8 | 1.1 (3) | 119 | 861 |
| 40 | 0.9 | 1.1 (5) | 133 | 1125 | 0.3 | 0.9 (1) | 0.4 | 0.6 (4) | 0.4 | 0.6 (3) | 50 | 315 |
| 41 | 0.8 | 1.0 (5) | 120 | 1010 | 1.5 | 2.2 (4) | 1.2 | 1.4 (3) | 0.9 | 1.2 (3) | 136 | 1049 |
| 42 | 2.6 | 3.1 (5) | 452 | 3677 | 2.3 | 3.7 (1) | 2.1 | 2.6 (3) | 2.0 | 2.4 (2) | 356 | 2583 |

[a] Number between parenthesis represents the storey in which maximum SDR was recorded.
[b] Displacement measured from double integration of acceleration records.

406

407 ***4.2 Period***

408

409 Prior to the start of the experimental program, ambient vibrations were used to estimate the initial period
410 of the structure in both directions. For the unbraced building configuration, the estimated initial periods
411 were 0.36 s and 0.47 s in the NS and EW directions, respectively. "Effective periods $T_{eff}$" for each test
412 run were calculated using Eq. (1), where $T_o$ is an initial estimate of period, $K_o$ is the initial effective
413 stiffness of the structure, and $K_i$ is the effective stiffness calculated in each direction during each test
414 run. $T_o$ was calculated as the average time difference between consecutive high-amplitude peaks of the
415 roof displacement in each direction, recorded during the first test run using each building configuration
416 (i.e. run 1 for the unbraced configuration in the EW direction, run 8 for the braced configuration in the
417 EW direction, and run 2 for the NS direction). Effective stiffness was calculated as the slope of the
418 base-shear–CoM roof displacement curve connecting the point of maximum displacement to the origin,
419 as shown in Fig. 18. Estimates of the effective period for all test runs are shown in Fig. 19.

420

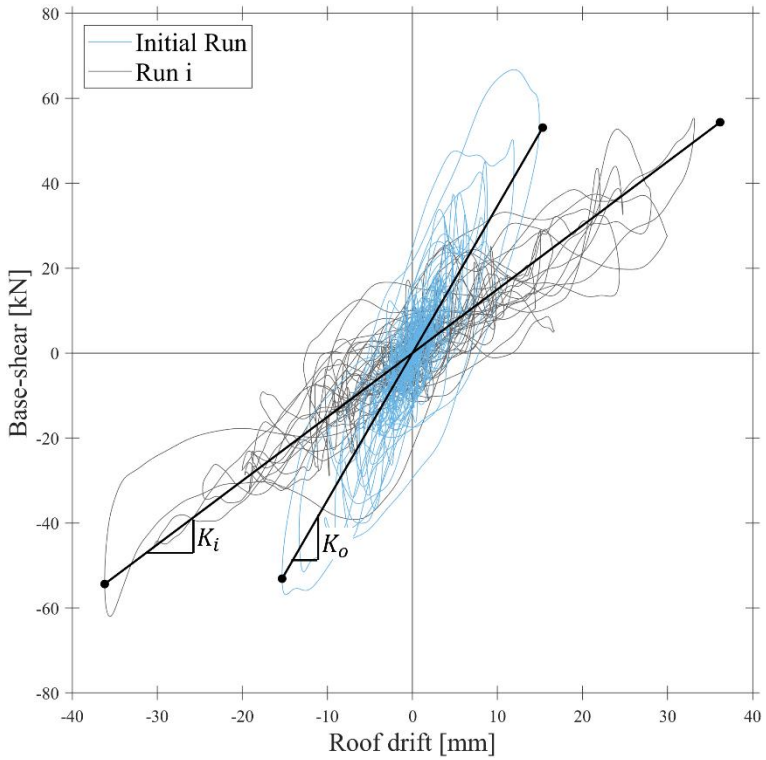



**Fig. 18.** Comparison of effective stiffness calculated at the initial run vs. effective stiffness calculated at a subsequent run i.

Effective periods were used to calculate spectral displacements of an equivalent single-degree-of-freedom (SDOF) system using measured ground accelerations for each test run. Damping ratio $\beta_{eff}$ for each run was calculated using Eq. (2), based on the ratio of the initial period $T_o$ to the effective period $T_{eff}$ (Gülkan & Sozen, 1974; Shibata & Sozen, 1974). Calculated damping ratios varied between 2% and 7%. SDOF displacements were projected to the roof displacement of a multi-degree-of-freedom system (MDOF) by multiplying it by the modal participation factor (Γ) and corresponding mode-shape factor (φ). Γ was taken equal to 1.1 for the unbraced configuration, 1.3 for the braced configuration, and 1.4 for the NS configuration, determined from the dominant mode in each case using a linear model of the test specimen with gross section properties. Mode-shape factors were normalized such that their value at the CoM on the top level was equal to 1. Estimated drifts were compared with measured maximum roof-drifts at the centre of mass (Fig. 20), showing good agreement. Measured roof-drifts in the NS direction were on average 20% larger than the estimated values, with a coefficient of variation (COV) of 0.2. Measured roof-drifts in the EW direction for the unbraced configuration were on average 8% smaller than estimations, with a COV of 0.3, while for the braced configuration, measured values in the EW direction were on average 17% larger than their estimated counterparts, with a COV of 0.3.

These drift estimates had better correlation with measured drifts than spectral displacements calculated using the estimated initial period of the structure or other measures of ground motion intensity, such as PGV.

$$T_{eff} = T_o \sqrt{\frac{K_o}{K_i}} \tag{1}$$

$$\beta_{eff} = 0.2 \cdot \left( 1 - \frac{1}{\left(\frac{T_{eff}}{T_o}\right)^{1/4}} \right) + 0.02 \tag{2}$$

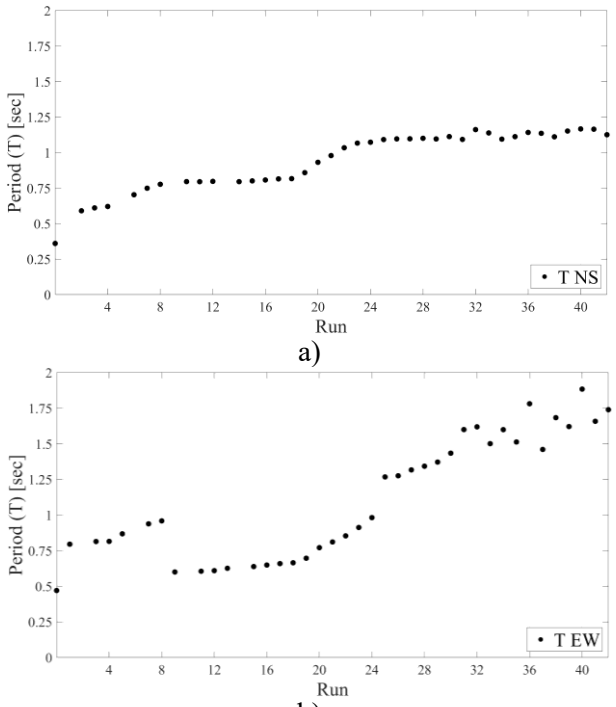



**Fig. 19.** Effective periods in a) NS direction, and b) EW direction.

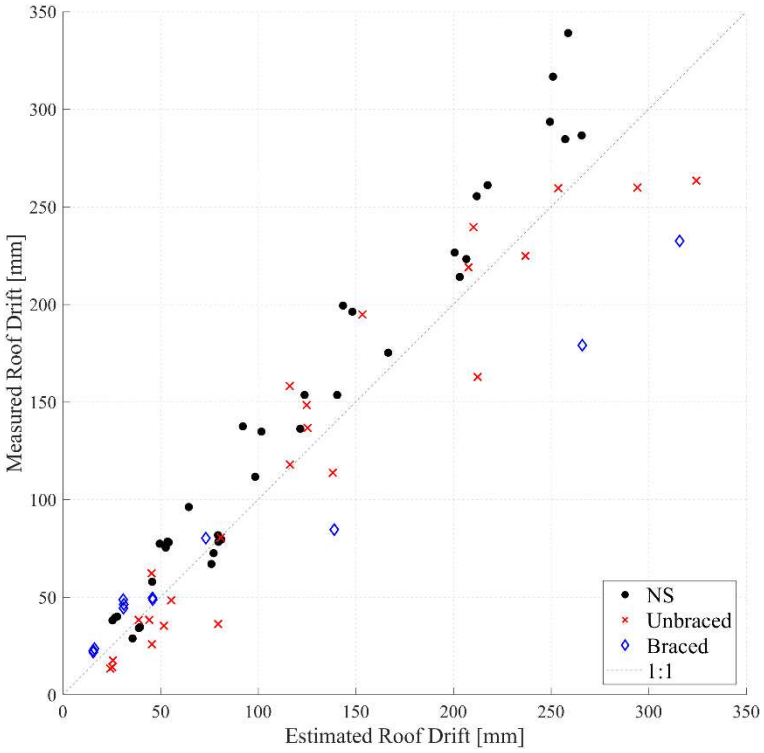



**Fig. 20.** Estimated vs. measured peak roof drift at CoM.

442

443 ***4.3 Base shear***

444

445 Base shear was calculated based on the story weights and recorded floor accelerations at the centre of
446 mass. Measured base shear coefficients $C_b$, calculated as the ratio of maximum base-shear to building
447 weight, are plotted against RDRs at the centre of mass in Fig. 21, where approximately trilinear
448 envelopes were fitted to the data. For the NS direction and the EW direction with an unbraced
449 configuration, as shown in Figs 16(a) and 16(b), the base shear coefficients reached maximum around
450 0.6 and 0.5 at RDR of 1.5% and 1.0%, respectively, while for the EW direction with a braced
451 configuration, the maximum base shear coefficient recorded was 0.7 at a RDR of 1.8%. The height of
452 the resultant force remained nearly constant at two-thirds of the total height of the building during the
453 whole experimental program.

454

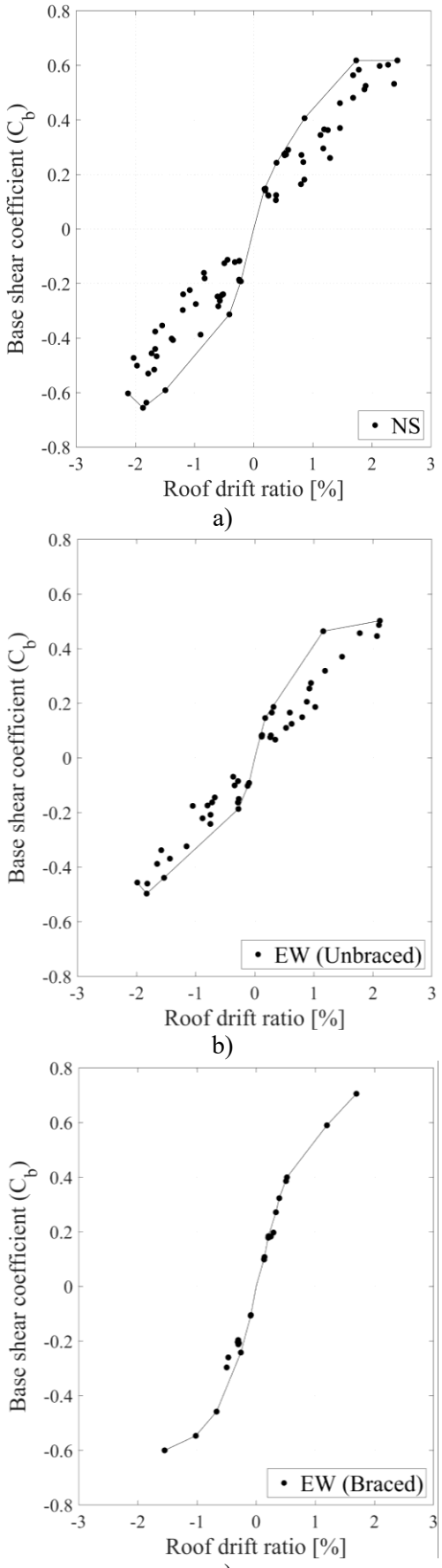



**Fig 21.** Base shear coefficient envelopes for a) NS direction, b) unbraced configuration in EW direction and c) braced configuration in EW direction.

### *4.4 Response of structural elements*

*RC elements*

Crack maps of the floor slab at the 2nd story and roof slab are presented in Fig. 22. Before the commencement of tests, cracks with widths smaller than 0.55 mm were observed in the slabs, due to shrinkage and the lifting and installation processes. During testing, cracks tended to form along lines connecting the inner corners of the RC wall and steel columns. More cracks formed over supporting beams along gridlines B and C. The maximum permanent crack width measured after completion of all tests was 0.9 mm along gridline B. Spalling was observed at the north slab-wall interface on several stories. Reinforcement was not exposed as a consequence of spalling (Fig. 23). Crack patterns of the RC coupled walls in the 1st story are presented in Fig. 24. Distributed cracks along the full height of the 1st storey developed during run 6, reaching a SDR of nearly 0.6%. The maximum permanent crack width measured after the tests was 0.5 mm, located near the top of the foundation. Nearly all wall cracking occurred in the first storey.

For the coupling beams, diagonal cracking initiated during test runs reaching a SDR of nearly 0.6% in the EW direction. After test run 24, which reached a maximum SDR of 2.9% in the EW direction, multiple diagonal cracks and corner concrete crushing was observed at the 1st and 3rd storey coupling beams. Maximum permanent crack width measured after this test was 6 mm, observed on the exterior face of the 3rd storey coupling beam, as shown in Fig. 25(a). Damage to the coupling beams did not result in discernible increases in drift. To prevent additional damage to the exterior 3rd storey coupling beam, it was strengthened after test run 28, using four sets of steel clams consisting of 40-mm thick steel plates connected by 10 mm threaded rods, as shown in Fig. 25(b). The steel clamps were tightened to a snug-tight condition. Crack width measured after the installation of the clamps was 0.3 mm and remained relatively constant until the removal of the clamps before test run 42. These results suggest

that the exterior clamps used were an effective repair alternative. After the end of the experimental program, the maximum measured crack width on the coupling beams was approximately 2 mm. Other than the damage observed in this coupling beam, the details used in the structure resulted in no brittle or unexpected failure modes.

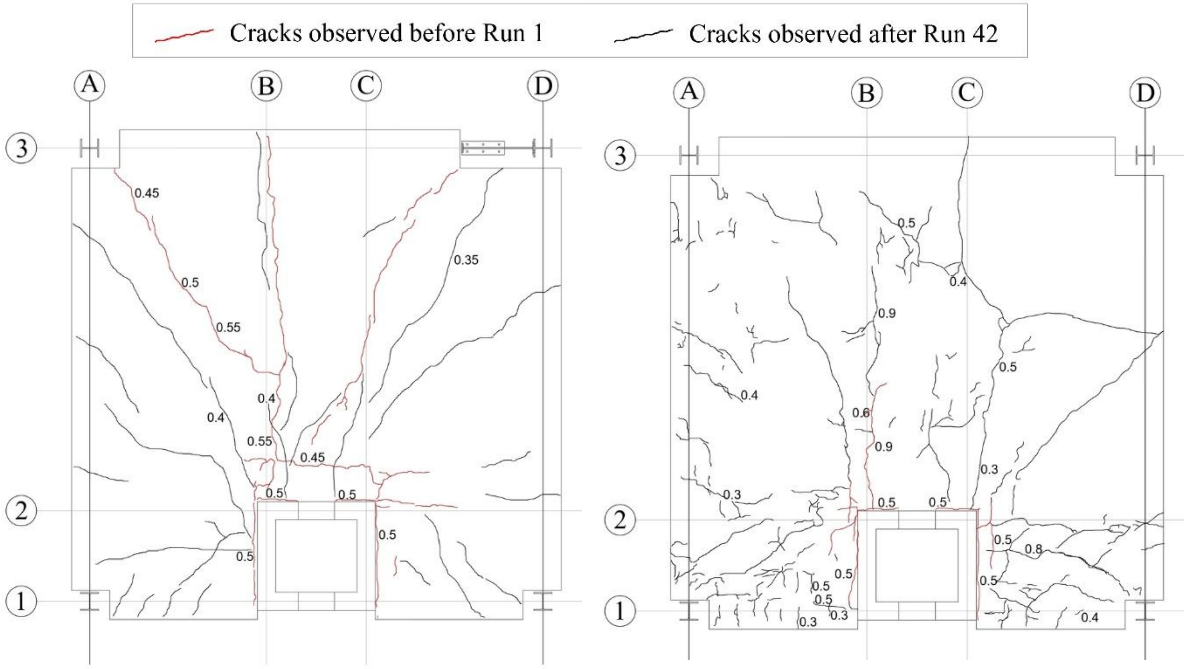



**Fig. 22.** Crack patterns of a) slab of 2nd story and b) roof slab.



**Fig. 23.** Photographs of spalling observed at the north slab-wall interface in the 2nd storey

488
489

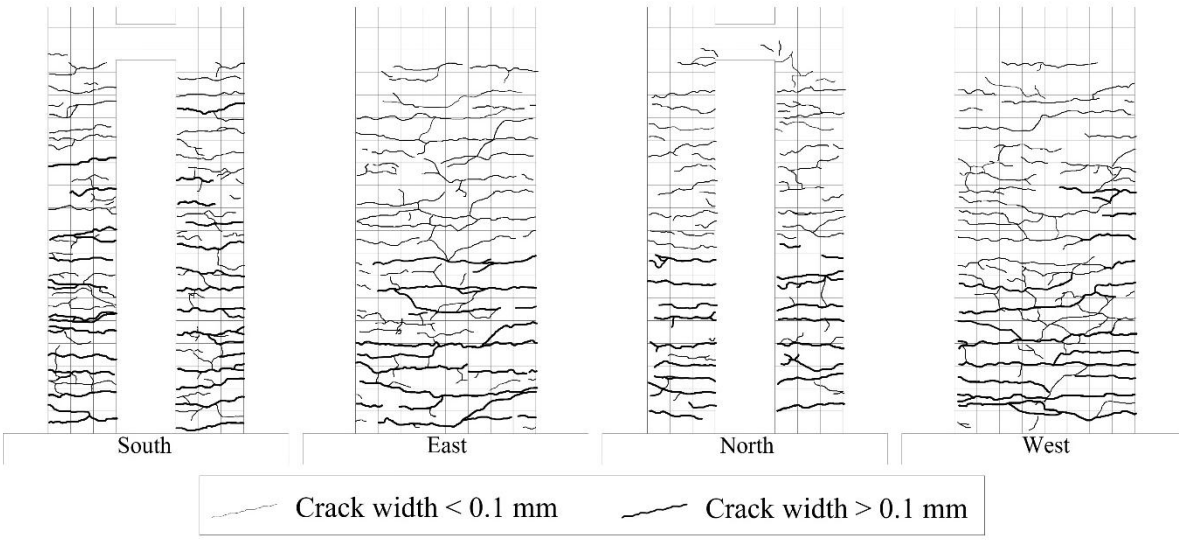
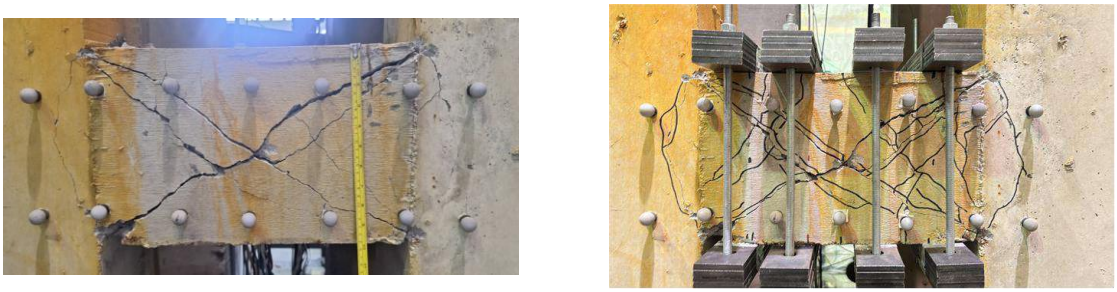



**Fig. 24.** Crack pattern of RC coupled wall at 1st story.

490
491



a) b)

**Fig. 25.** Coupling beam at 3rd storey: a) cracks after test run 24, and b) repaired coupling beam after test run 28.

492

493 *Steel elements*

494

495 No damage was observed in any steel element throughout the experimental program. Signs of yielding
496 near the base of the columns were first observed during test run 31 with a PGV of 80 cm/s. No relative
497 displacements were observed in the steel beam-wall connections, even though the connection had
498 slotted holes, implying that the coupling between the bolts on the steel beams and slabs effectively
499 increased the rotational stiffness and strength of these connections. In Phase 2, yielding of the braced
500 frame concentrated exclusively in the sBRBs. No signs of yielding were observed in gusset plates,
501 beams, or columns. Yielding of the core plate of the sBRBs was only observed for the test runs with
502 SDR larger than 0.6%. Maximum tensile strains on the core plates were recorded during the test run 24
503 and equal to 0.19%, 0.32%, 0.30%, and 0.26% for the sBRBs on 1st, 2nd, 3rd, and 4th story, respectively,
504 while the corresponding maximum compressive strains were 0.25%, 0.32%, 0.28%, and 0.22%.

505

506 ***4.5 Response of non-structural elements***

507

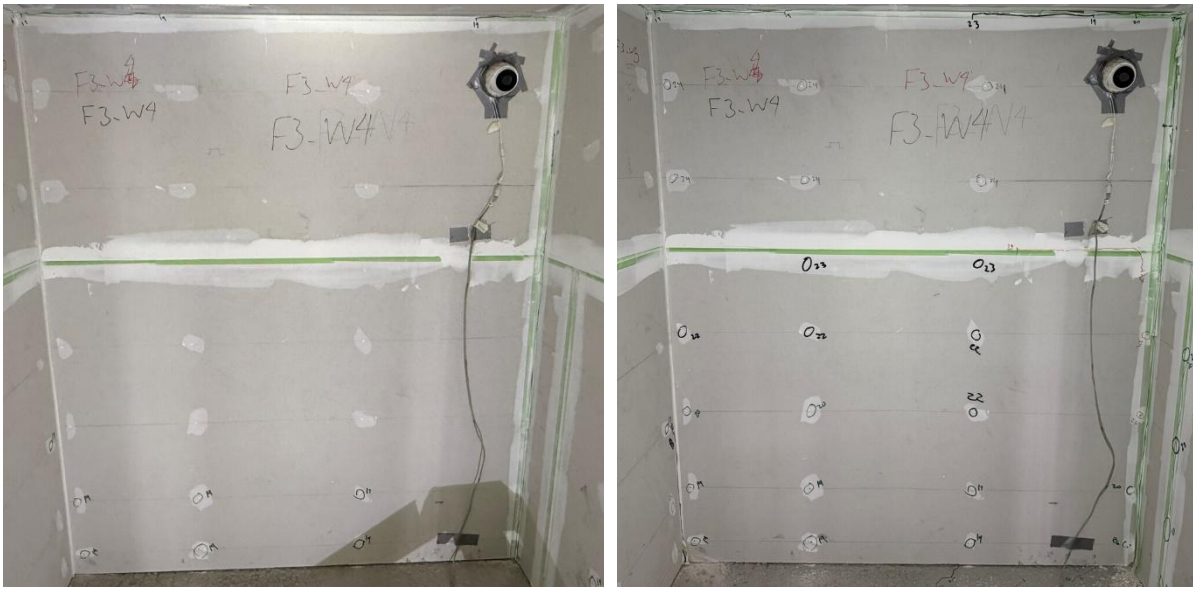
508 Damage deemed to be repairable was observed in all rooms except for the east room on the 2nd story
509 for SDRs smaller than approximately 1%. Damage was characterized by hairline cracks around door
510 openings, warping of joint paper tape at corner joints and at the wall-to-ceiling interface, and screw
511 impressions concentrated near the base track of all partition walls, as shown in Fig. 26(a). Once SDR
512 surpassed 1%, screw impressions were observed along the full height of the partition walls, plasterboard
513 dislodged from studs, and local buckling of studs was observed, as shown in Fig 26(b). Damage states
514 of all rooms suggest that above an SDR of 1.5%, replacement of partition walls may be necessary. Fig.
515 27 shows the progression of screw impressions per unit length of each wall in the second and third
516 storeys as function of the maximum past SDR.

517

Damage of the concealed and fully floating ceiling was concentrated around their perimeter, where minor separation cracking and localized plasterboard crushing was observed. No damage was observed in the fire sprinkler piping system across the experimental program. This was likely a consequence of the short hanger lengths (250 mm) and the reduced weight of the system, as it was not pressurized with water or other fluids.

Limited screw impressions on the lower half of the T-shaped partition walls of the fourth storey were observed between SDRs of 1% and 2%. Local buckling of the edge studs was also observed within this range. The performance of these partition walls was likely enhanced by the gap provided at the top of the plasterboard. At SDRs above 2%, distortion of the partition walls closed the gap, causing them to detach from their connections to the slabs above and below. In one case, SDRs above 2% resulted in the collapse of a T-shaped partition wall, as shown in Fig. 28.

The response of the appliances in the east room on the second storey and the library bookshelves on the fifth storey was quantified based on the rate of fallen objects from their original positions. These items are generally classified to be 'acceleration-sensitive', suggesting that a higher rate of fallen objects would be expected during the tests with the braced configuration. Fig. 29 shows a comparison of fallen books on the fifth storey after test 21, in which the braced configuration was used, and after test 29, in which the unbraced configuration was used. Peak floor accelerations measured during these tests were 1.7 g, and 1.2 g, respectively. Nevertheless, the rate at which objects fell from their original position was similar for both tests. The same trend of was observed throughout the experimental program: the amount of fallen objects was relatively insensitive to the building configuration used.




a) b)

**Fig. 26.** Damage progression on the south partition wall of the west room on the third floor observed after a) test run 19, reaching a maximum SDR of 1%, and b) test run 24, reaching a maximum SDR of 2%.

541

542

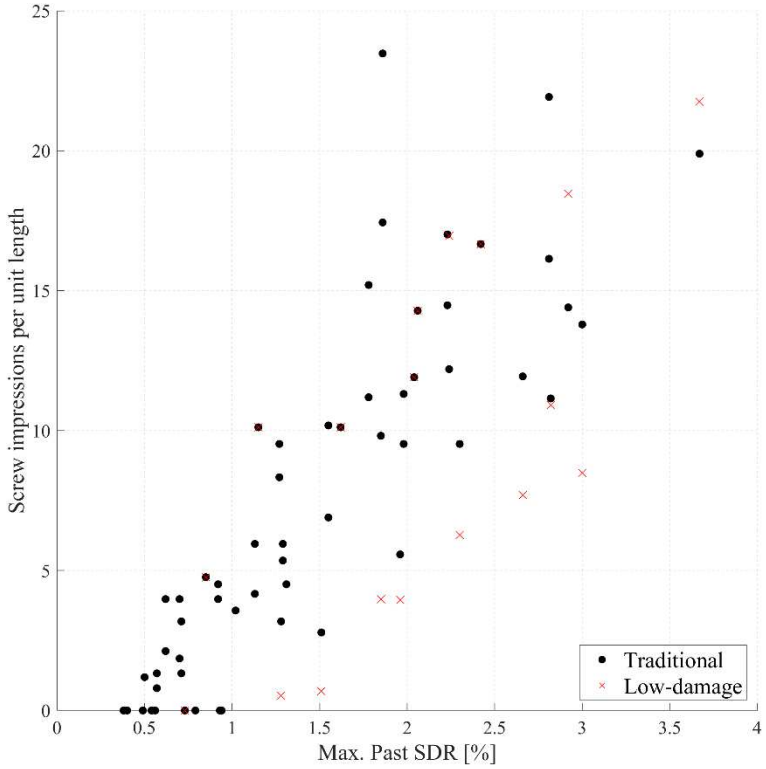
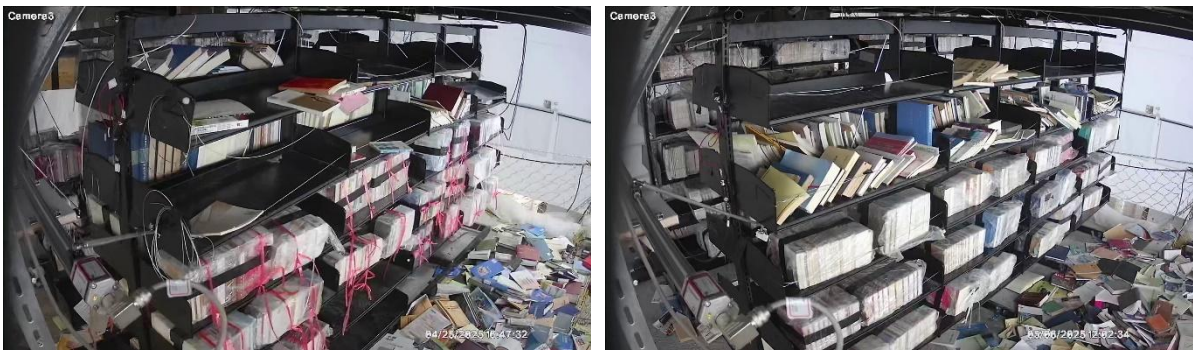



**Fig. 27.** Progression of screw impressions per unit length on the partition walls on the second and third storeys as function of maximum past SDR.

543




**Fig. 28.** Collapsed T-shaped partition wall.




a) b)

**Fig. 29.** Comparison of fallen books from the shelves located on the fifth storey of the test specimen during a) test run 21, and b) test run 29.

## 5. Conclusions

A structural steel–reinforced concrete hybrid building was subjected to 42 simulated earthquake motions. Two building configurations (braced and unbraced) were included in the experimental program to evaluate the effects of building irregularity and drift on the performance of structural and non-structural elements. Key conclusions are summarized here:

1. The details used resulted in a structure exhibiting no brittle or unexpected failures, even after being subjected to peak roof-drift ratios of 3% and storey-drift ratios of 3.8%.
2. Peak roof-drift ratios and storey-drift ratios were nearly proportional to PGV for test runs completed using the El Centro ground motion. The rate of increase of drift for tests using other

ground motions was also proportional to PGV, with the main difference being that larger drift demands were observed for the same intensity, suggesting sensitivity to the shape of the displacement spectrum.

3. For motions repeated at a given ground motion intensity, and for roof drift ratios larger than 0.5%, roof drift was on average 10% larger in later tests.
4. Maximum displacements at the centre of mass were dominated by the first mode of response of the test specimen in each direction. Instances of peak displacement in one direction were usually simultaneous with near zero displacements in the perpendicular direction.
5. Spectral displacements calculated based on estimates of effective period and effective damping were linearly proportional to peak roof drifts measured at the centre of mass of the test specimen. Spectral displacements calculated based on estimates of effective period had better correlation with measured roof drifts than spectral displacements calculated based on estimates of initial period or other measures of ground motion intensity.
6. Damage to partition walls was assessed as repairable for storey-drift ratios not exceeding 1%. Damage under this limit consisted of hairline cracks around the perimeter of the plasterboard, and screw impressions near the lower track of each partition wall.
7. The rate of fallen objects in the east room on the second storey and in the library shelves in the fifth storey was independent of the building configuration used, even though recorded peak floor accelerations were higher when the braced configuration was used.

## Acknowledgements

The authors gratefully acknowledge the technical and financial support provided by the New Zealand Centre for Earthquake Resilience Te Hiranga Rū (QuakeCoRE), the National Center for Research on Earthquake Engineering (NCREE), National Institutes of Applied Research, Taiwan, and industry partners including HILTI, Rondo, and Thermosash

The authors would also like to thank everyone involved in the planning and execution of the tests.

## References


Abrams DP, Sozen MA (1979) Experimental Study of Frame-Wall Interaction in Reinforced Concrete Structures Subjected to Strong Earthquake Motions. Civil Engineering Studies, Structural Research Series No. 460. University of Illinois at Urbana-Champaign.

Algan BB (1982) Drift and Damage Considerations in Earthquake-Resistant Design of Reinforced Concrete Buildings. Dissertation, University of Illinois at Urbana-Champaign.

Aristizabal-Ochoa JD, Sozen MA (1976) Behavior of Ten-Story Reinforced Concrete Walls Subjected to Earthquake Motions. Civil Engineering Studies. Structural Research Series No. 431. University of Illinois at Urbana-Champaign.

Bonacci JF (1989). Experiments to Study Seismic Drift of Reinforced Concrete Structures. Dissertation, University of Illinois at Urbana-Champaign.

Bruneau M, MacRae G (2017) RECONSTRUCTING CHRISTCHURCH: A Seismic Shift in Building Structural Systems.

Cecen H (1979) Response of Ten Story, Reinforced Concrete Model Frames to Simulated Earthquakes. Dissertation, University of Illinois at Urbana-Champaign.

El-Tawil S, Harries, KA, Fortney PJ, Shahrooz BM, Kurama Y (2010) Seismic Design of Hybrid Coupled Wall Systems: State of the Art. Journal of Structural Engineering, 136(7), 755–769. https://doi.org/10.1061/ASCEST.1943-541X.0000186

Gülkan P, Sozen MA (1974) Inelastic Responses of Reinforced Concrete Structures to Earthquake Motions. *ACI Journal*, 604–610.

Hawkins NM, Mitchell D, Roeder CW (1980) Moment Resisting Connections for Mixed Construction. Engineering Journal, 17(1), 1–10.

Healey TJ, Sozen MA (1978) Experimental Study of the Dynamic Response of a Ten-Story Reinforced Concrete Frame with a Tall First Story. Civil Engineering Studies, Structural Research Series No. 450. University of Illinois at Urbana-Champaign.

Hou G, Chen B, Miao Q, Liu X, Huang J. (2008) DESIGN AND RESEARCH ON COMPOSITE STEEL AND CONCRETE FRAME-CORE WALL STRUCTURE.

Hung CC, Lu WT (2017) A Performance-Based Design Method for Coupled Wall Structures. Journal of Earthquake Engineering, 21(4), 579–603. https://doi.org/10.1080/13632469.2016.1172379

Ko DW, Lee HS (2006). Shaking table tests on a high-rise RC building model having torsional eccentricity in soft lower storeys. Earthquake Engineering and Structural Dynamics, 35(11), 1425–1451. https://doi.org/10.1002/eqe.590

Lepage A (1996) Seismic Drift Estimates for RC Structures. 11th World Conf. on Earthquake Engineering, Canadian Association for Earthquake Engineering.

Liu A, Zhou D (2005) Experimental study on seismic behavior of semi-rigid connection between steel beam and concrete wall. Earthquake Engineering and Engineering Vibration, 4(1), 129–137. https://doi.org/10.1007/s11803-005-0031-x

Moehle JP, Sozen MA (1978) Earthquake Simulation Tests of a Ten-Story Reinforced Concrete Frame with a Discontinued First-Level Beam. Civil Engineering Studies, Structural Research Series No. 451. University of Illinois at Urbana-Champaign.

Moehle JP, Sozen MA (1980) Experiments to Study Earthquake Response of Reinforced Concrete Structures with Stiffness Interruptions. Civil Engineering Studies, Structural Research Series No. 482. University of Illinois at Urbana-Champaign.

Newmark N (1973) A Study of Vertical and Horizontal Earthquake Spectra.

Pascua C, Henry R, Toma C (2023) Review of Recently Constructed Concrete Wall- Steel Frame Hybrid Buildings. Bulletin of the New Zealand Society for Earthquake Engineering, 56(2), 91–103. https://doi.org/10.5459/bnzsee.1602

Pascua C, Henry R, Toma C, Clifton, C (2023) Experimental Tests on Concrete Wall-Steel Beam Connections. Building for the Future: Durable, Sustainable, Resilient. Proceedings of the Fib Symposium, 1712–1721.

Pledger L (2025) The Effects of Reducing Design Drift Limits for Structures. Dissertation, University of Canterbury.

Pujol S, Irfanoglu A, Puranam A (2022) Drift-Driven Design of Buildings; Mete Sozen's Works on Earthquake Engineering.

Roeder CW, Hawkins NM (1981) Connections Between Steel Frames and Concrete Walls. Engineering Journal, 18(1), 22–29.

Shah PP (2021) Seismic Drift Demands. Dissertation, Purdue University.

Shahrooz BM, Deason JT, Tunc G (2004) Outrigger Beam-Wall Connections. I: Component Testing and Development of Design Model. Journal of Structural Engineering, 130(2), 253–261. https://doi.org/10.1061/ASCE0733-94452004130:2253

Shahrooz BM, Tunc G, Deason, JT (2004) Outrigger Beam-Wall Connections. II: Subassembly Testing and Further Modeling Enhancements. Journal of Structural Engineering, 130(2): 262-270. https://doi.org/10.1061/ASCE0733-94452004130:2262

Shibata A, Sozen MA (1974) The Substitute-Structure Method for Earthquake-Resistant Design of Reinforced Concrete Frames. Civil Engineering Studies, Structural Research Series No. 412. University of Illinois at Urbana-Champaign.

Sozen MA (1980) Review of Earthquake Response of Reinforced Concrete Buildings with a View to Drift Control. Seventh World Conference of Earthquake Engineering.

Sozen, MA (2013) Why Should Drift Drive Design for Earthquake Resistance? Proceedings of the 6th Civil Engineering Conference in Asia Region: Embracing the Future through Sustainability.

Suzuki T, Puranam AY, Elwood KJ, Lee HJ, Hsiao FP, Hwang SJ (2021) Shake table tests of seven-story reinforced concrete structures with torsional irregularities: Test program and datasets. Earthquake Spectra, 37(4), 2946–2970. https://doi.org/10.1177/87552930211016869

## Statements & Declarations


### *Funding*

This work was supported by by the New Zealand Centre for Earthquake Resilience Te Hiranga Rū (QuakeCoRE), the National Center for Research on Earthquake Engineering (NCREE), National Institutes of Applied Research, Taiwan, and industry partners including HILTI, Rondo, and Thermosash.


### *Competing Interests*

The authors have no relevant financial or non-financial interests to disclose.

### *Author Contributions*

All authors contributed to the study conception, design, and data collection. Data analysis was performed by Alejandro Saenz Calad, Yu-Hsin Cheng, and Mojtaba Hosseini. The first draft of the manuscript was written by Alejandro Saenz Calad and all authors commented on previous versions of the manuscript. All authors read and approved the final manuscript.

### *Data Availability*

The datasets generated and analysed during the current study are available in the Datacenterhub repository, https://datacenterhub.org/post-nees.html